TALLINNA ÜLIKOOL
Matemaatika ja loodusteaduste instituut
Loodusteaduste osakond

Maria Kesa

THE EFFECT OF DORSAL HUMP SIZE ON THE HYDRODYNAMIC DRAG OF THE SOCKEYE SALMON (*ONCORHYNCHUS NERKA*) AND THE CONFLICT BETWEEN NATURAL AND SEXUAL SELECTION

Bakalaureusetöö

Juhendaja: Prof. Maarja Kruusmaa
PhD Madis Listak
MSc Jaas Ježov

Autor:..... "...." .....2009. a
Juhendaja:..... "...." .....2009. a
Lubatud kaitsmisele:..... "..." .....2009. a
Õppetooli juhataja.....

Tallinn 2009

SISUKORD

0. TÖÖ REFERATIIVNE KOKKUVÕTE EESTI KEELES

Seljaküüru suuruse mõju Alaska punase lõhe (*Oncorhynchus nerka)* hüdrodünaamilisele takistusjõule ning konflikt loodusliku ja sugulise valiku vahel

SISSEJUHATUS

Alaska punane lõhe (*Oncorhynchus nerka)* on semelpaarne lõheline. Sellel liigil väljendub seksuaalne dimorfism nende rände ajal ookeanist mageveelisesse kudemispaika. Isased kasvatavad endale suured seljaküürud ja lõuad, emased aga ei muuda oma kuju, jäädes voolujooneliseks. Isase seljaküüru suurust soosib suguline valik. Antud lõputöö eesmärgiks on uurida eksperimentaalselt seksuaalse dimorfismi mõju isase lõhe hüdrodünaamilisele tõhususele. Ma võtan hüpoteesiks, et suuremaga küüruga isenditel on suurem hüdrodünaamiline takistusjõud. Sellisel juhul suureneb ka ujumise energiakulu ning loomulik valik hakkab toimima selle vastu, sest Alaska punasel lõhel on teel kudemispaika piiratud energiavarud, mille ammendamisel kala sureb. Simulatsiooni tulemused kinnitasid antud hüpoteesi ja näitasid, et suurema küüruga kalad peavad ujumiseks kulutama rohkem energiat.

0.1. Alaska punase lõhe bioloogia

Käesolevas lõputöös uurin ma morfoloogia mõju Alaska punase lõhe (*Oncorhynchus nerka)* isaste hüdrodünaamilisele efektiivsusele. Alaska punane lõhe on anadroomne[1] ja semelpaarne[2] lõheline, kes elutseb Vaikse ookeani põhja osas, Põhja-Jaapanist kuni Beringi

[1] Anadroomsed kalad veedavad enamuse oma elust ookeanis, kuid paljunevad magedas vees.
[2] Semelpaarsed liigid paljunevad elus vaid korra ja surevad pärast paljunemist.

mereni ja Californiani (fishbase). Seda liiki on uuritud põhjalikult tema majandusliku tähtsuse ja tugiliigi staatuse tõttu (Hinch et al 2006). Samuti pakub see liik huvi omapärase elukäigu seisukohalt. Nendel lõhelistel väljendub seksuaalne dimorfism nende rände ajal ookeanist mageveelisesse kudemispaika (kusjuures iga populatsioon tuleb paljunema samasse kudemispaika, kus selle isendid sündisid). Isased kasvatavad endale suured seljaküürud ja lõuad, emased aga ei muuda oma kuju, jäädes voolujooneliseks (joonis 1). Küüru kasvatamine ja lõugade pikenemine toimub isastel läbi kõhre ladustamise (Hendry ja Berg 1999), mis on tehtud valgust. Selleks kasutatakse lihase valku, kuna rasva varusid ei saa teisendada valguks. Rasva varusid kasutatakse liikumiseks (Hendry ja Berg 1999).

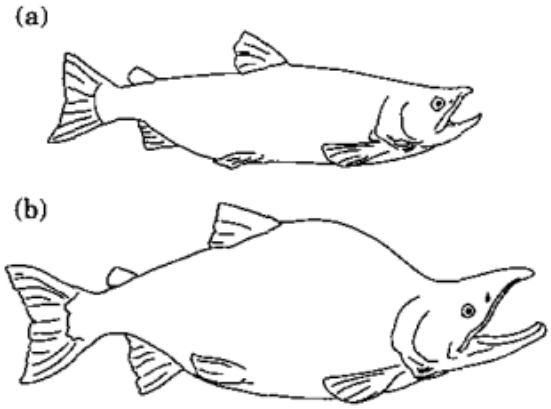

Joonis 1. Emane (a) ja isane (b) Alaska punane lõhe seksuaalse dimorfismi avaldumise ajal migratsioonil kudemispaika (võetud Quinn ja Foote 1994).

Isase seljaküüru on uuritud sugulise valiku seisukohalt. Vaatlusandmete statistiline töötlus näitab, et emased eelistavad paljuneda isastega, kellel on suuremad küürud (Quinn ja Foote 1994; Hamon ja Foote 2005). Samuti on uuritud seljaküüru suuruse varieeruvust erinevates populatsioonides. Need uuringud on näidanud, et populatsioonides, kus ränne kudemispaika on raskem (st teekond on pikem või vee vool on kiirem), on isastel keskmiselt väiksemad seljaküürud ja voolujoonelisemad kehad (Crossin et al 2004; Hamon ja Foote 2005). Lahtiseks aga on jäänud küsimus, kuidas küüru kasvatamine mõjutab isase hüdrodünaamilist takistusjõudu, mis omakorda mõjutab tema liikumisele kuluva energia vajadust.

See küsimus huvitab mind, sest Alaska punane lõhe saab paljuneda vaid korra elus ja pärast paljunemist ta sureb. Kui nad jõuavad magedasse vette, et sooritada oma viimane teekond kudemispaika, lõpetavad nad söömise. Seega nad peavad sooritama teekonna, mis on

mõnede populatsioonide puhul enam kui 1000 km pikk, piiratud energiavarudega. Energiavarude ammendumisel kala sureb. Keha konsistentsi uuringud on näidanud, et kala sureb, kui energia varud langevad alla 4MJ/kg (Crossin et al 2003). Individuaaltelemeetria uuringud on näidanud, et umbes 25% magedasse vette jõudnud lõhelistest surevad teel kudemispaika (Cooke et al 2006). Osa suremusest teekonnal on tingitud energiavarude enneaegsest otsasaamisest (Rand ja Hinch 1998; Cooke et al 2006). Võib juhtuda ka nii, et kalad jõuavad küll kudemispaika, ent kui nad on teekonnal liiga palju energiat ära tarvitanud, siis nad ei paljune (Cooke et al 2006). Seega on tõhus energia kasutamine sellele liigile esmase tähtsusega. Kuna isendid, kes ei jõua kudemispaika, ei paljune ja seega ei päranda oma geene järgmisele põlvkonnale, soosib looduslik valik kalu, kellel on energeetiliselt tõhusad liikumisviisid ja morfoloogia.

Sellise loodusliku valiku toime avaldub fenotüüpilises varieerumises populatsioonide vahel. Populatsioonidel on erinev migratsiooni raskus, mis sõltub migratsiooni pikkusest, jõe voolukiirusest ja turbulentsusest, karude jahtimisest jne. See tähendab seda, et loodusliku valiku surve energeetilisele tõhususele erineb erinevates populatsioonides. Eespool oli mainitud, et keha sügavuse ja keha pikkuse suhte morfoloogiline analüüs erinevates populatsioonides on näidanud, et lõhedel on populatsioonides, millel on raskem teekond, lühemad ja voolujoonelisemad kehad (Crossin et al 2004) ning et isased sellistes populatsioonides kasvatavad keskmiselt väiksemaid seljaküüre (Hamon ja Foote 2005). Ma sean hüpoteesiks, et seljaküür suurendab hüdrodünaamilist takistusjõudu. Sellisel juhul suureneb ka ujumise energiakulu ning loomulik valik hakkab toimima selle vastu, sest nendel lõhelistel on teel kudemispaika piiratud energiavarud.

Sugulisel ja looduslikul valikul on seega küüru suuruse suhtes vastupidine mõju. Suur küür mõjutab positiivselt isase võimalust paljuneda, kuid suurema küüruga isenditel on ka suurem risk surra energia puuduse tõttu. Alaska punase lõhe populatsioonid jaotuvad isase küüru keskmise suuruse suhtes vastavalt sellele kummal valiku tüübil on antud populatsiooni isenditele rohkem mõju.

Oma lõputöös ma uurin, kuidas isase seljaküür mõjutab tema hüdrodünaamilisi omadusi. Seljaküüru energeetilise hinna määramiseks kasutan ma füüsikalist ja arvutuslikku meetodit. Järgmine alampeatükk kirjeldab lühidalt kalade ujumise füüsikat.

0.2. Kalade ujumise füüsikaline taust

Võrreldes õhuga on vesi tihedam, kõrgema viskoossusega ja kokkusurumatu vedelik. Seetõttu jõud, mida vesi keskkonnana organismidele avaldab, on oma magnituudilt suuremad, kui need, mis mõjuvad organismidele õhu keskkonnas ning see mõjutab oluliselt seda, kuidas organismid selle keskkonnaga kohastunud on—nende liikumise mehhanismid ja energeetika on erinevad õhus elavate organismide omast. Joonisel 2 on kujutatud ujuvale kalale mõjuvad jõud.

Joonis 2. Jõud, mis mõjuvad liikuvale kalale (võetud Lane et al 1998).

Vee kokkusurumatuse tõttu paneb kala liikumine vees teda ümbritseva vee liikuma ning vee liikumine omakorda mõjutab kala (Lane et al 1998). Kala ujumine toimub läbi impulsi ülekande kala kehalt veele. Impulsi ülekanne on vee mass, mille kala keha liikumine on kiirendanud teatud keskmise kiiruseni. Impulsi ülekande kiirus määrab kindlaks edasilükke jõu, mida kala liikumine loob (Biewener 2003). Edasilükke jõud on esitatav valemina:

$$T = \frac{mu}{t}, \tag{1}$$

kus T (N) on edasilükke jõud, m (kg) on mass, u (m/s) on kiirus ja t (s) on aeg.

Töö, mida kala peab tegema, et ujuda teatud vahemaa konstantse edasilükke jõuga, on esitatav valemina:

$$W = T \cdot d, \tag{2}$$

kus W (J) on töö ja d (m) on läbitav vahemaa.

Vedelik avaldab vastupanu edasilükke jõule ja mõjutab kala keha vastassuunalise jõuga. Vedeliku takistavat mõju kehale nimetatakse takistusjõuks. Et kala saaks paigast liikuda, peab edasilükke jõud olema võrdne või suurem kui takistusjõud.

Üks faktor, millest takistusjõud sõltub, on vedeliku viskoossus. Kuna vesi on viskoossem kui õhk, nõuab vees liikumine suuremat võimsust. See on põhjus, miks takistusjõudu vähendavad adaptatsioonid on kaladele isegi tähtsamad kui lindudele—nad võivad potentsiaalselt palju enam energiat kaotada takistusjõu tõttu kui linnud antud liikumiskiiruse juures.

Bioloogid on uurinud liikuvatele organismidele mõjuvat takistusjõudu, et leida vastuseid küsimustele nende eluviiside kohta, adaptatsiooni kohta oma elukeskkonnaga ning et arvutada nende liikumise energeetilist kulukust. Seda on tehtud kasutades tuule- ja veetunneleid, et mõõta jõudusid, mis organismidele mõjuvad (Pennycuick et al 1988; Sagnes et al 2000; Lovvorn et al 1991; Lovvorn et al 2001; Shelley ja Vogel 2000; Puijalon et al 2005), kasutades video tehnikaid, et mõõta liuglevate veeloomade negatiivset kiirendust (aeglustumist) (Bilo ja Nachtigall 1980; Stelle et al 2000) või kasutades modeleerimise tehnikaid (Miller et al 2004). Kõikides nendes uurimusmeetodites mõõdetakse jäiga keha takistusjõudu. Liikuvaid organisme ümbritsevat voolu on uuritud, kasutades arvutusliku hüdrodünaamika simulatsioone (Liu et al 1996; Liu et al 1997; Wolfgang et al 1999; Zhu et al 2002; Borazjani ja Sotiropoulos 2008, 2009). Oma lõputöös kasutan arvutusliku hüdrodünaamika simulatsioone, et uurida voolu Alaska punase lõhe isaste jäikade 3D mudelite ümber. See võimaldab mul kindlaks määrata erineva küüru suurusega isaste kehadele mõjuvat takistusjõudu. Järgmises alampeatükis kirjeldan ma oma simulatsioonide metoodikat.

0.3. Metoodika

Ma rakendan arvutusliku hüdrodünaamika simulatsioone, et uurida seksuaalse dimorfismi mõju isase lõhe hüdrodünaamilisele tõhususele. Arvuti simuleerib veevoolu erinevate küüru suurustega kala mudelite ümber ja arvutab nende mudelite hüdrodünaamilist takistusjõudu. Seda tehakse nelja erineva voolukiiruse juures. See eksperiment võimaldab mul kindlaks määrata, kuidas küüru suurus on seotud hüdrodünaamilise takistusjõuga, mis mõjub kala kehale. Selles alampeatükis kirjeldan ma lühidalt oma simulatsioonide metoodikat.

0.3.1. Kala mudeli valmistamine

Isase Alaska punase lõhe 3D mudel oli võetud Toucani virtuaalsest muuseumist (ToucanMuseum). Mudelid olid loodud Alaska punase lõhe fotograafide järgi (e-maili vahetus mudeli loojaga toco04@toucan.co.jp). Ma muutsin mudeleid kasutades 3D modelleerimise programmi Blender 2.48-t. Ma eemaldasin mudelilt kõik uimed peale sabauime ja skaleerisin mudeli 60 cm pikkuseks (mudeli ninatipust kuni saba otsani). Ihtüoloogid mõõdavad kala pikkust silmast kuni kala selgroo viimase sabapoolse luuni. Sellise mõõtmisviisi järgi olid mu mudelid 46.5 cm pikad.

Ma muutsin astmeliselt mudeli küüru suurust. Tulemuseks sain 5 mudelit, mis olid identsed kõikides aspektides peale küüru suuruse. Nendel mudelitel on seega erinev kehasügavus (vertikaalne pikkus küüru otsast kõhuni, mis on risti keha horisontaal pikkusega). Keha pikkuse ja sügavuse jagatist nimetatakse ristmõõtmete suhteks. Tabelis 1 on toodud mudelite kehasügavused, ristmõõtmete suhted ja mudelite pindalad. Ma kasutasin keha pikkuse mõõduna ihtüoloogide mõõtmisviisi. Pindalad olid mõõdetud kasutades Blender MeasureMesh skripti. Joonisel 3 on näidatatud kaks mudelit.

Keha sügavus (cm)	Ristmõõtmete suhe	Pindala (cm^2)
21.00	2.21	1750.50
19.50	2.38	1719.78
18.00	2.58	1670.12
16.50	2.82	1591.53
15.00	3.10	1520.35

Tabel 1. Mudelite mõõtmed

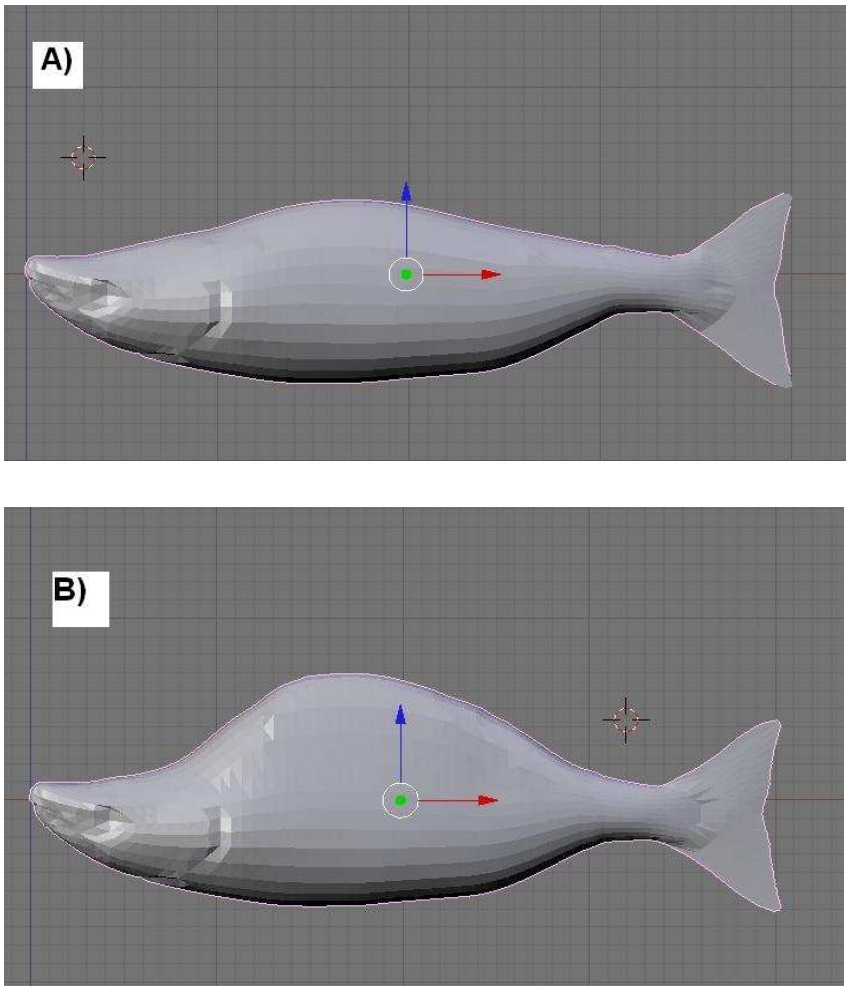

Joonis 3. Alaska punase lõhe 3D mudelid ristmõõtmete suhtega A) 3.10 ja B) 2.38.

0.3.2. Arvutusliku hüdrodünaamika simulatsioonid

Arvutuslik hüdrodünaamika on vedelike mehaanika haru, mis rakendab numbrilisi meetodeid ja algoritme, et lahendada vedelike voolamisega seotud probleeme. Ma kasutasin avatud lähtekoodiga arvutusliku hüdrodünaamika programmi OpenFOAM. Simulatsioonid olid tehtud lõplike ruumalade meetodiga (Finite Volume Method, FVM) ja turbulentsi modeleerimisel Reynoldsi keskmistatud Navier-Stokesi võrranditega (Reynolds averaged Navier-Stokes, RANS).

Arvutuslik hüdrodünaamika baseerub kolmel fundamentaalsel füüsikalisel printsiibil, mis valitsevad vedelike voolamist: massi jäävuse seadus, Newtoni teine seadus ja energia jäävuse seadus[3]. Need füüsikalised printsiibid väljendatakse matemaatiliste võrrandite abil. Siin on nad esitatud Descartesi tensor tähistuse abil:

$$\frac{\partial u_i}{\partial x_i} = 0 \tag{3}$$

$$\frac{\partial u_i}{\partial t} + u_j \frac{\partial u_i}{\partial x_j} = -\frac{1}{\rho}\frac{\partial p}{\partial x_i} + \upsilon \frac{\partial^2 u_i}{\partial x_j^2} \tag{4}$$

$$\frac{\partial e_0}{\partial t} + u_j \frac{\partial e_0}{\partial x_j} = -\frac{1}{\rho}\left[u_j \frac{\partial p}{\partial x_j} + \frac{\partial q_j}{\partial x_j} \right] + \upsilon u_i \frac{\partial^2 u_i}{\partial x_j^2} \tag{5}$$

kus υ (m^2/s) on kinemaatiline viskoossusus, ρ (kg/m^3) on tihedus, e_0 (J) on koguenergia ja q (W/m^2) on soojusvool.

Arvuti arvutab nende võrrandite numbrilised lahendused simulatsiooni domeeni (simulatsiooniruumi) igas punktis. Selle jaoks simulatsiooniruum diskretiseeritakse (jaotatakse) väikesteks elementideks. Diskretiseeritud simulatsiooniruumi nimetatakse meshiks ehk võreks. Joonisel 4 on näidatud diskretiseeritud kala mudel. Minu simulatsioonides oli domeenis 1.3 miljonit elementi. Simulatsiooni tulemuseks saadakse voolu parameetrite (kiirus, rõhk jne) väljad diskreetsetel ajasammudel.

[3] Kuna antud eksperimendis temperatuuri ülekanne ei ole tähtis, siis ma eeldan, et temperatuur on konstantne. Võrrand (5) ei oma seega antud simulatsioonis tähtis.

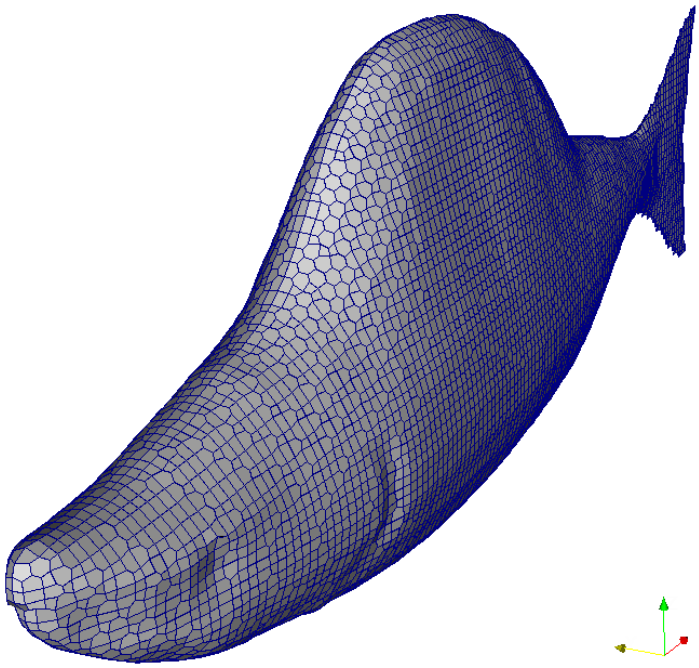

Joonis 4. Diskretiseeritud kala mudel (mesh).

0.3.3. Takistusjõu ja takistuskoefitsendi arvutamine

Takistusjõud x1 suunas arvutatakse integreerides rõhk ja viskoossed jõud, mis mõjuvad kehale selles suunas:

$$D = \int_A (-pn_1 + \tau_{1j} n_j) dA . \qquad (6)$$

kus p on rõhk (N/m^2), n_i on ühik normaalvektori i-s komponent pinnal dA ja τ_{ij} on viskoosse stressi tensor.

Takistuskoefitsent on dimensioonitu suurus, mis näitab kuidas kuju mõjutab takistusjõudu. Seda suurust arvutatakse vastavalt eksperimentaalsetele takistusjõu tulemustele iga voolukiiruse juures. Seda arvutatakse järgmise valemiga:

$$C_d = \frac{D}{\frac{1}{2}\rho A U^2}, \tag{7}$$

kus A on mudeli pindala (toodud tabelis 1) ja U on simulatsiooni voolukiirus.

0.4. Tulemused

0.4.1. Takistusjõud ja takistuskoefitsendid

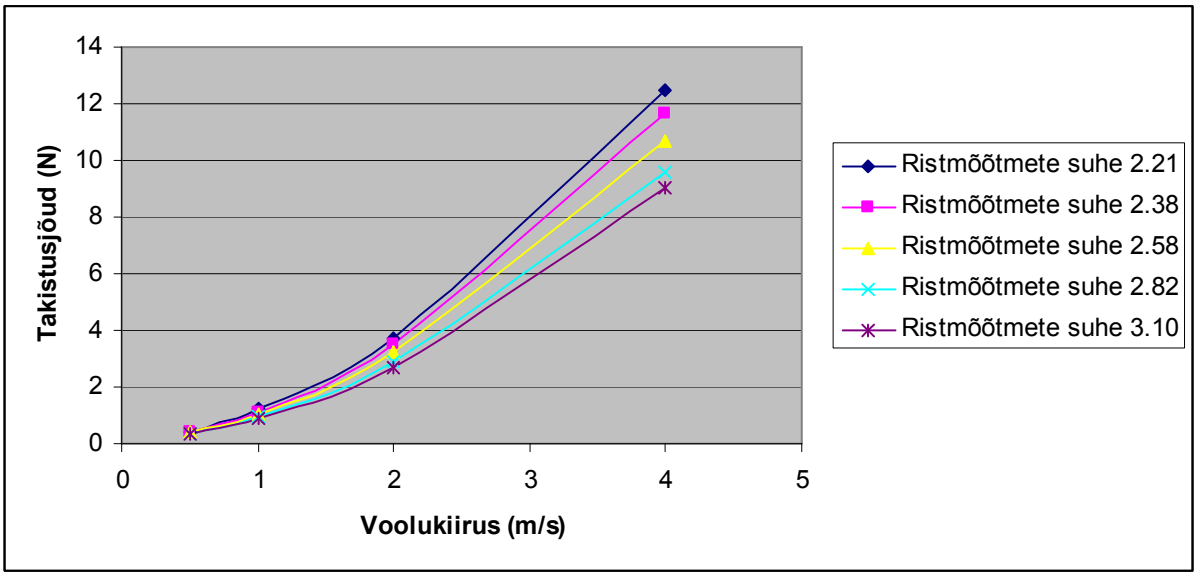

Joonis 5. Takistusjõu sõltuvus voolukiirusest

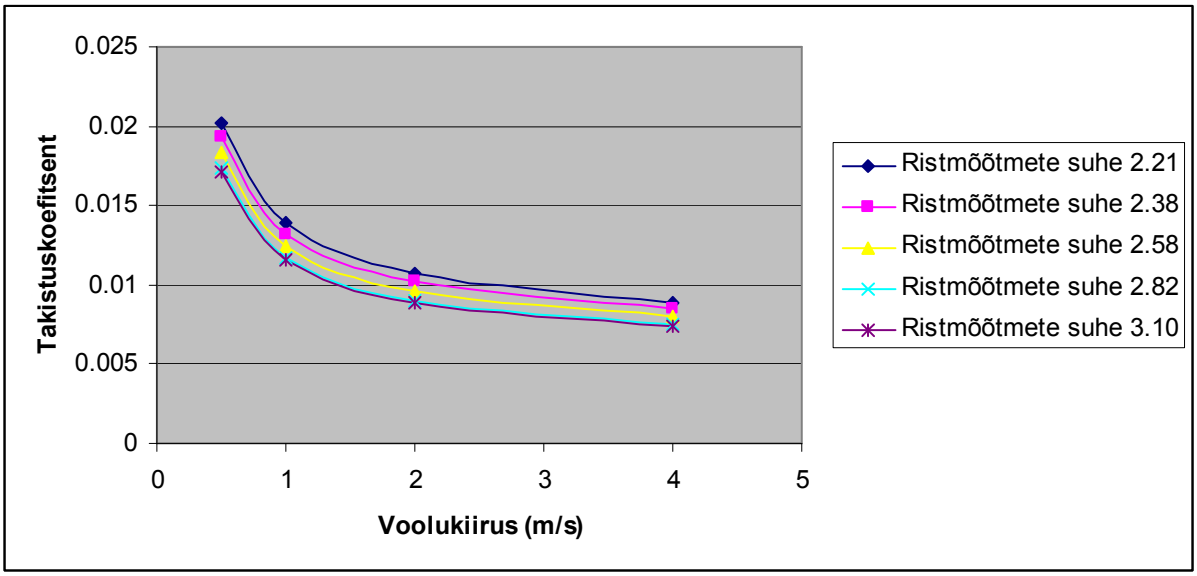

Joonis 6. Takistuskoefitsendi sõltuvus voolukiirusest

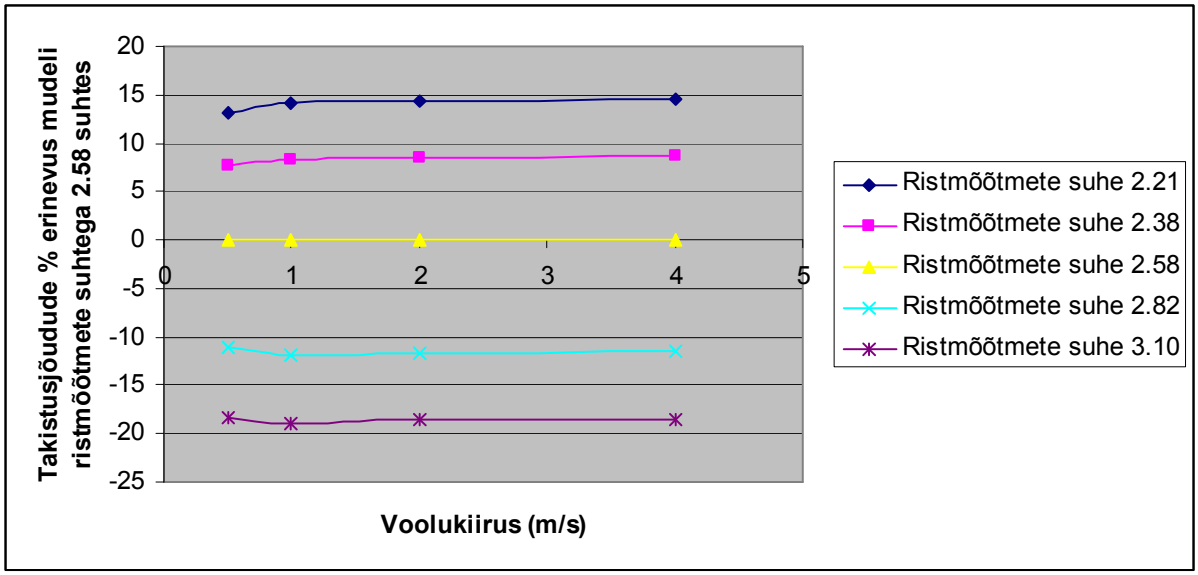

Joonis 7. Takistusjõudude protsentuaalne erinevus mudeli ristmõõtmete suhtega 2.58 suhtes.

0.4.2. Energeetika arvutused

Et ujuda, peab kala tekitama vähemalt nii palju edasilükke jõudu, et see oleks võrdne takistusjõuga. Sellest lähtudes olid energeetika arvutused tehtud kasutades valemeid (1) ja (2).

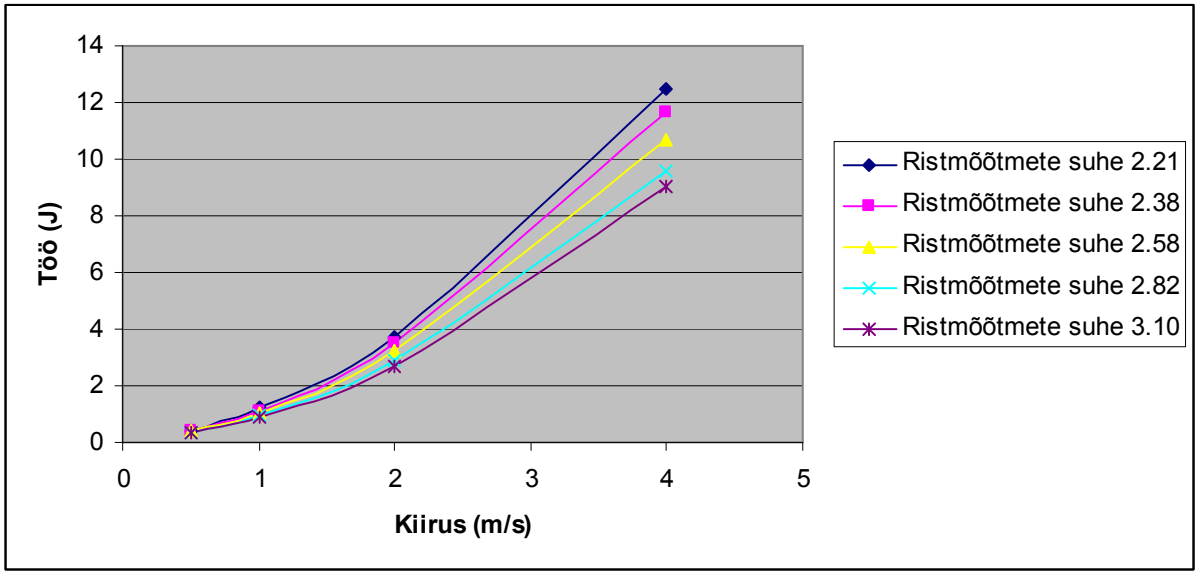

Joonis 8. Töö, mida kala peab tegema, et ujuda 1 m antud kiirusel[4]

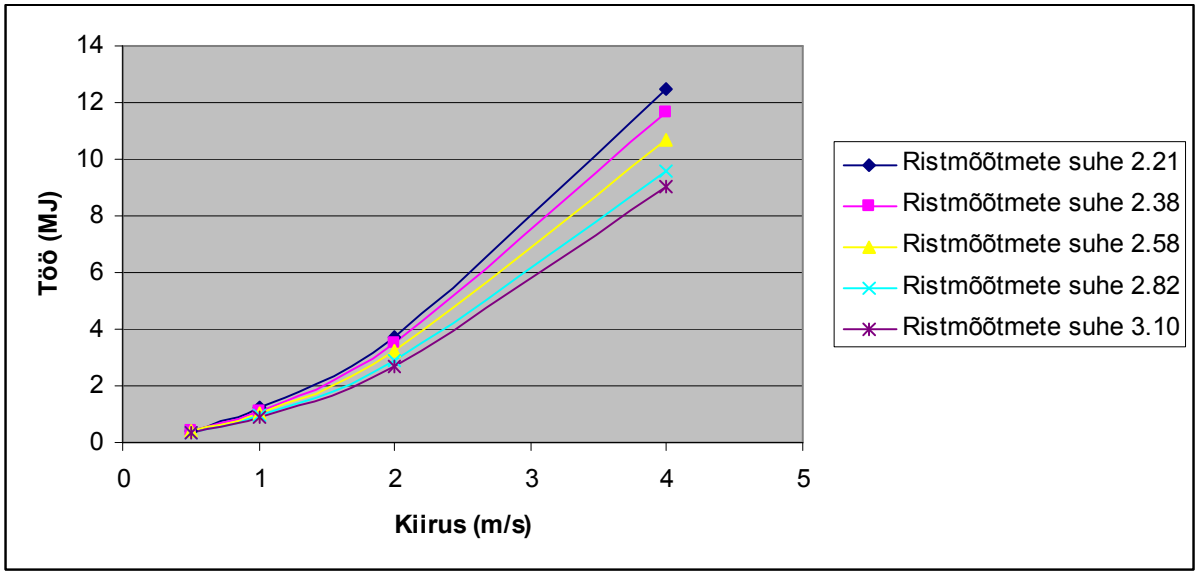

Joonis 9. Töö, mida kala peab tegema, et ujuda 1000 km antud kiirusel

[4] Kiiruse all me mõtleme kala kiirust vedeliku suhtes. Taustsüsteemi võib siduda vedeliku või kalaga, see ei muuda simuleeritud andmete füüsikalist sisu.

0.4.3. Voolu visualisatsioonid

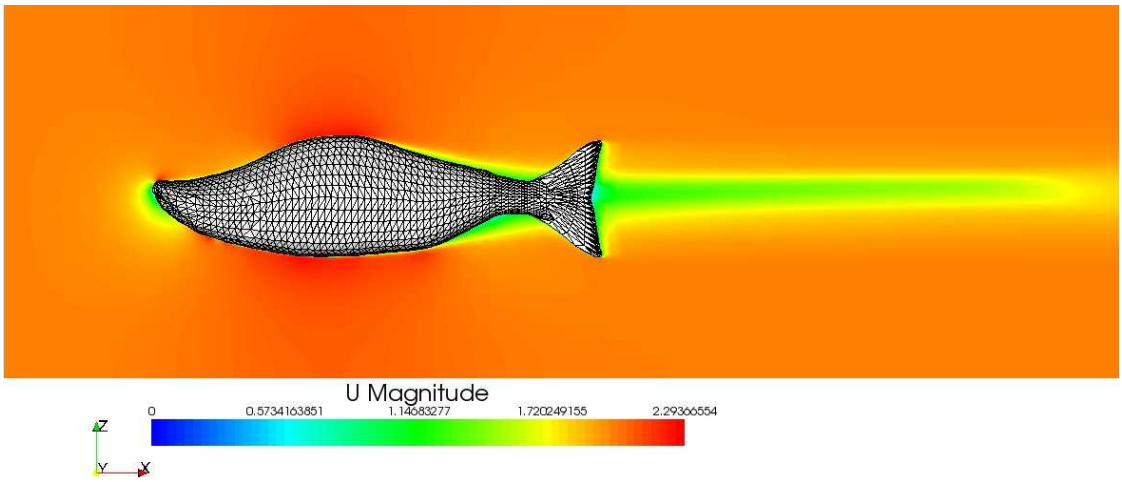

Joonis 10. Kiirusväli ümber lõhe mudeli ristmõõtmete suhtega 2.82 simulatsiooni kiirusel 2 m/s. Graafiku ribal on ühikuteks m/s.

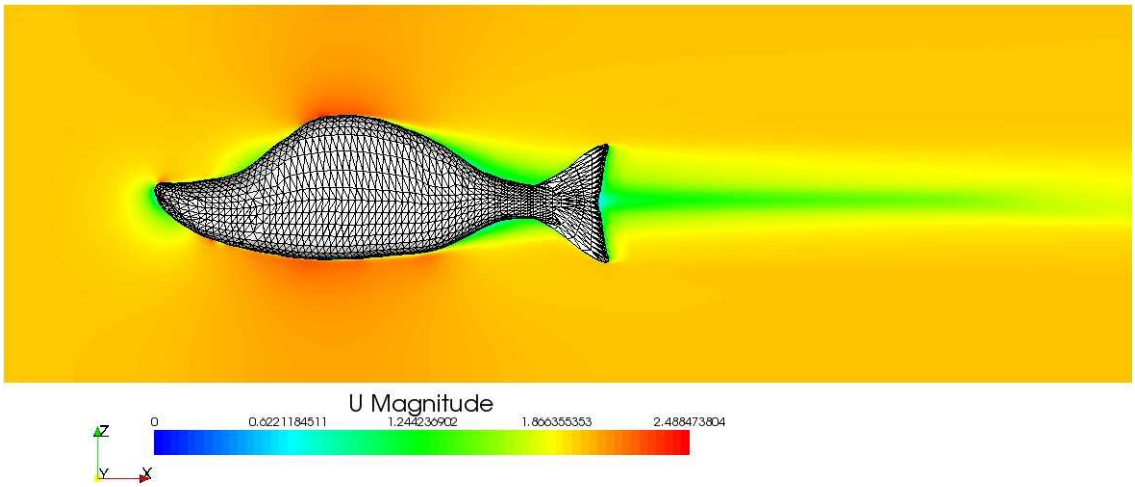

Joonis 11. Kiirusväli ümber lõhe mudeli ristmõõtmete suhtega 2.38 simulatsiooni kiirusel 2 m/s. Graafiku ribal on ühikuteks m/s.

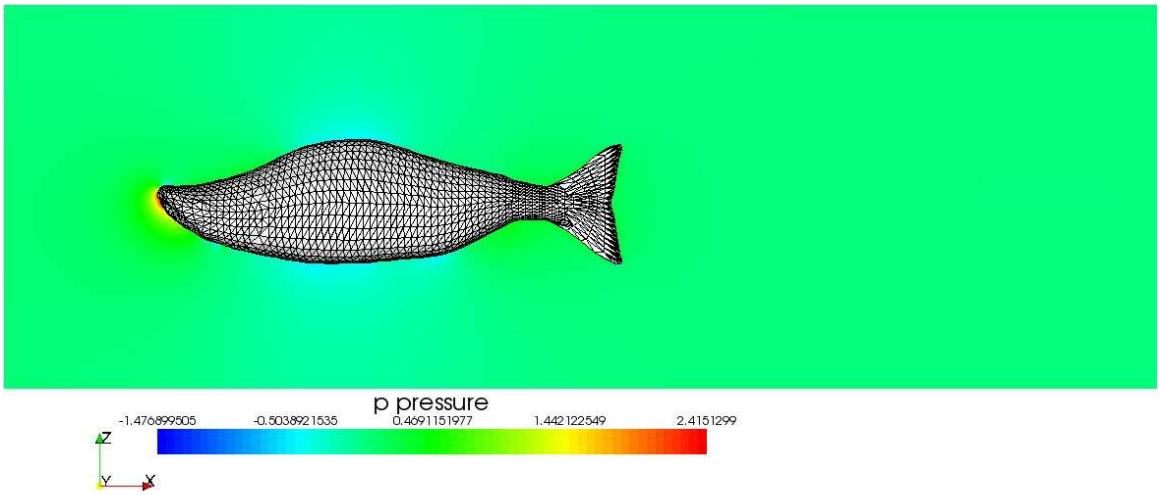

Joonis 12. Rõhuväli ümber lõhe mudeli ristmõõtmete suhtega 2.38 simulatsiooni kiirusel 2 m/s. Graafiku ribal on ühikuteks Pa.

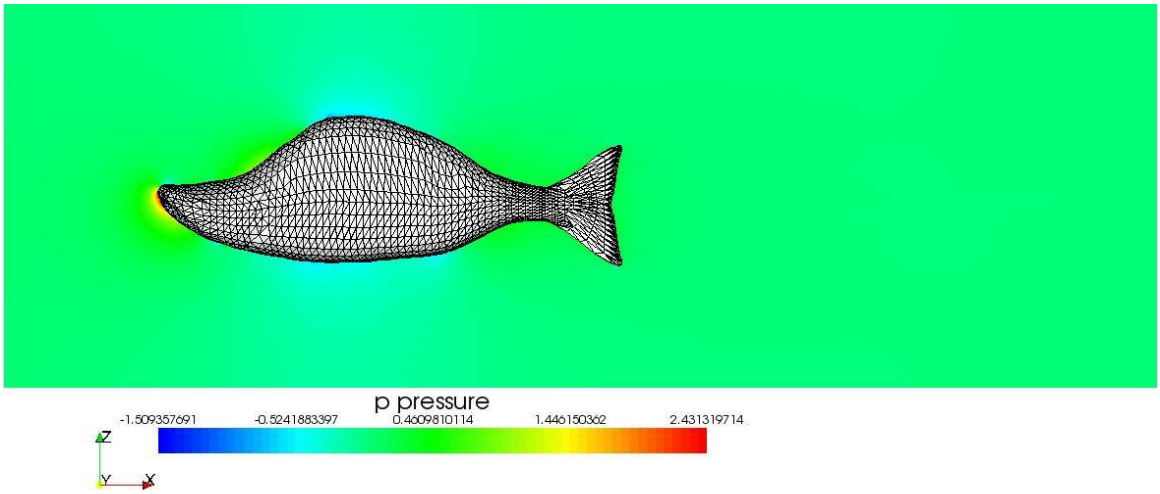

Joonis 13. Rõhuväli ümber lõhe mudeli ristmõõtmete suhtega 2.38 simulatsiooni kiirusel 2 m/s. Graafiku ribal on ühikuteks Pa.

0.5. Järeldus

Simulatsioonid näitasid, et suurema küüruga kalale mõjub suurem hüdrodünaamiline takistusjõud iga simuleeritud voolukiiruse juures. Takistuskoefitsendid näitasid, et takistusjõu muutus küüru kasvatamisest ei ole tingitud mitte ainult keha pindala suurenemisest vaid ka kujumuutusest (küüruga kala keha on hüdrodünaamiliselt vähem efektiivne). Need tulemused tõestasid seatud hüpoteesi, et suuremate küürudega isased peavad ujumiseks ületama suurema takistusjõu. Joonis 7 näitab, et kõige suurema küüruga (kõige madalama ristmõõtmete suhtega) mudelile mõjus ligikaudu 35% suurem takistusjõud võrreldes kõige väiksema küüruga voolujoonelise (kõige korgem ristmõõtmete suhtega) mudeliga. See tähendab, et suurima küüruga kala peab sama vahemaa ujumiseks kasutama 35% rohkem energiat kui väikseima küüruga kala (sest töö on takistusjõud korrutatud vahemaaga).

Kuna turbulents simulatsioonis olid arvutatud Reynoldsi keskmistatud Navier-Stokesi võrranditega turbulentsi, mis keskmistab rõhu ja teisi voolu parameetreid. Seetõttu peenemaid voolu struktuure nagu keeriselisust ei ole voolu simulatsioonist näha. Kuid nende visualisatsioonide põhjal on ikkagi võimalik teha üldisi järeldusi voolu iseloomust. Joonisel 11 kujutatud mudelil on suurem hüdrodünaamiline jälg, kui joonisel 10 kujutatud mudelil. Sellest võib järeldada, et suurema küüruga mudel moonutab voolu enda ümber rohkem kui väiksema küüruga mudel. Seega peab talle mõjuma ka suurem takistusjõud.

KOKKUVÕTE

Selle lõputöö keskne küsimus on: kuidas mõjutab seljaküür isase Alaska punase lõhe hüdrodünaamilisi omadusi? Sellele küsimusele on kolm võimalikku vastust: suurem küür võib takistusjõudu suurendada, vähendada või muutmata jätta. Minu hüpoteesiks oli, et küür suurendab takistusjõudu seega suurendades ka lõhe energeetilisi kulutusi. Selle hüpoteesi kontrollimiseks kasutasin arvutuslikku hüdrodünaamikat simuleerimaks voolu erineva küürusuurustega mudelite ümber erinevatel voolukiirustel. Simulatsiooni tulemustest selgus, et suuremale küürule vastab suurem takistusjõud ja takistusjõu koefitsent iga voolukiiruse korral. See tõestas lõputöös püstitatud hüpoteesi.

Suurema takistusjõu tõttu peab suurema küüruga isane liikumisele rohkem energiat kulutama. Kuna suured küürud on soositud sugulise valiku poolt, siis on suurenenud energia tarbimine "hind", mida suurema küüruga isane maksab eelise eest paljunemisel. Energia aga on selles elujärgus Alaska punastele lõhedele piiratud ressurss, sest need lõhelised lõpetavad söömise, kui nad magedasse vette sisenevad. Kui energia tarbimine jõuab 4MJ/kg, siis need lõhelised surevad. Seega võib suurema küüru poolt tekitatud energeetiline lisahind osadele isenditele osutuda liiga kulukaks ja nad surevad kurnatusse enne, kui jõuavad kudemispaika.

Lõputöös kasutatud füüsikaline meetod oli efektiivne seljaküüru hüdrodünaamilise rolli selgitamisel. Füüsika (biomehhaanika) tähtsus erinevates bioloogia valdkondades kasvab, sest see võimaldab analüüsida organismi toimimise füüsikalisi aluseid, mis toob endaga kaasa uut perspektiivi arusaamaks, kuidas organismid kohanevad oma keskkonnaga, kasutavad oma energeetilisi ressursse ning kuidas liigid evolutsioneeruvad.

INTRODUCTION

Sockeye salmon (*Oncorhynchus nerka*) is a semelparous species of salmon that expresses extensive sexual dimorphism during migration from the ocean to freshwater spawning grounds. While females of this species remain streamlined, the males grow large dorsal humps and extended jaws. The size of the dorsal hump is strongly correlated with mating success. Statistically it has been shown that females prefer males with larger dorsal humps, thus they are favored by sexual selection.

However, the average hump size of a sockeye male varies in different populations and is related to the difficulty of the migration to the spawning grounds. Males in populations with more difficult migrations have on average smaller dorsal humps.

The aim of this thesis is to investigate experimentally the effect of the hump size on the hydrodynamic efficiency of the sockeye male. I hypothesize that the increase in hump size also leads to an increased hydrodynamic drag (resistive force exerted by the fluid on a swimming fish). If that is indeed the case then the energetic demand of swimming will also increase. Then increase in hump size will be opposed by natural selection, because sockeye salmon have a limited energetic budget as they stop eating upon entering freshwater. Sexual and natural selection for hump size would then be in opposition. Populations of sockeye salmon will then differentiate with respect to male hump size according to which selective pressure dominates in that population.

To study the drag of sockeye salmon a biomechanical approach is adopted. Biomechanical approach to the study of organisms can elucidate the nature of the physical relationship between the organism and its environment. Here the morphology of sockeye salmon is studied using a modern engineering method and employing physics to progress our knowledge of the biology of this species.

1. SOCKEYE SALMON (*ONCORHYNCHUS NERKA*) BIOLOGY

1.1. Life history of sockeye salmon

The sockeye salmon (*Oncorhynchus nerka*) is an anadromous species of fish belonging to the family Salmonidae, order Salmoniformes, class Actinopterygii. There are two forms, the anadromous form known as the sockeye and the landlocked form known as the kokanee (Fishbase). This thesis is concerned with the anadromous form of sockeye salmon, all of the future references will be to the anadromous form.

Sockeye salmon is found in the North Pacific ocean, from northern Japan to Bering Sea and to California, USA (Fishbase). This species has been studied extensively, because it is a keystone species and also of great economic importance (Hinch et al, 2006). The availability of extensive literature on the behavior, migration energetics and morphology of sockeye salmon allows the author to research this species without physical access to it. The aim of this chapter is to elucidate important aspects of sockeye biology. In this section the lifecycle of sockeye will be considered.

Sockeye's lifecycle consists of several directed migrations. Sockeye eggs develop and hatch in rivers or lakes. After hatching they go from spawning grounds to nursery lakes, where they spend 1 or 2 years feeding and growing. Some sockeye salmon populations spend only a few months in the lake rearing grounds, after which they go directly to lower river estuaries or the sea. These populations are dubbed ''sea-type'' sockeye salmon. Other populations rear in rivers for 1 or 2 years instead of lakes, these are called ''river-type'' sockeye salmon (Gustafson et al, 1997). After rearing sokeyes migrate downstream to the ocean. In the ocean they migrate offshore to the feeding grounds, where they spend 2-3 years. Sockeye salmon are philopatric, which means that at the end of their lifecycle they return to the place of their birth to reproduce. So when gonadal maturation is initiated, they start a directed return migration towards the coast. In the final phase of migration sockeye re-enter freshwater and migrate upriver to travel home to their natal stream or lake beach.

Sockeyes stop eating after entering freshwater, so they have a fixed energetic budget for the remainder of the journey (Brett, 1995; Standen et al, 2002; Hinch et al, 2006). On this journey their gonads ripen and they reach sexual maturity. They turn red and the development of secondary sexual characteristics takes place, with male sockeye salmon growing dorsal humps and elongated jaws (kypes) as illustrated in Figure 1.1. (Hinch et al, 2006). These secondary sexual characteristics play a role in ensuring reproductive success for males, as they are subject to sexual selection (Quinn and Foote, 1994; Hamon and Foote, 2005). When sockeye salmon reach their natal stream or lake beach they spawn. Sockeyes are semelparous, after spawning they die. As a consequence of philopatricity different sockeye salmon populations do not cross-reproduce, although a small amount of straying occurs between different populations with some individuals leaving their original population to spawn with another (Lin et al, 2008).

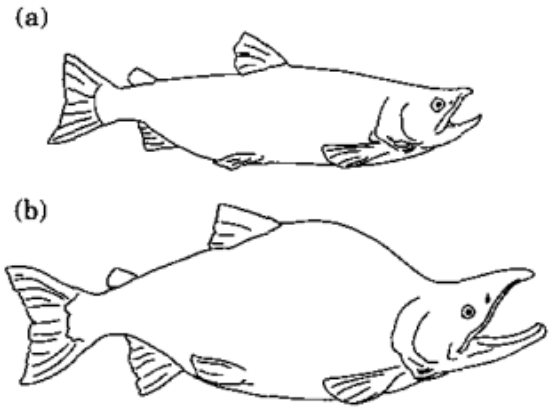

Figure 1.1. Female (a) and male (b) sockeye salmon during the last phase of migration and spawning, when sexual dimorphism becomes expressed (from Quinn and Foote, 1994).

This thesis is concerned with the last migration phase of the sockeye salmon, when the fish swim upriver to their natal stream or beach. The effect of the dorsal hump on the hydrodynamic efficiency of sockeye males will be investigated. As sockeye salmon are semelparous they have just one opportunity to swim upriver and reproduce, this journey is of critical importance. Upon reaching freshwater they stop eating and thus have to perform the journey that is in some cases more than 1000 km long on a limited energy budget (Hinch et al, 2006). Premature depletion of energy reserves is fatal. Crossin et al (2003) showed using body constituent analysis that in general when energy reserves decline below 4 MJ/kg sockeye salmon die. Energy efficiency is thus a matter of survival. Cooke et al

(2006) showed using individual telemetry on different sockeye salmon runs that 50% of individuals succeeded in entering the river (failure of osmoregulation was the main cause of death for the rest) and of these 75% reached the spawning grounds. Some of enroute mortality can be attributed exhaustion of energy reserves (Rand and Hinch, 1998; Cooke et al, 2006). Even if the fish do arrive on the spawning grounds, if they spent excessive energy during the migration, they die without spawning (Cooke et al, 2006).

Since the individuals who are not able to complete the upriver journey do not spawn and hence do not contribute their genes to the next generation, natural selection is likely to favor fish with energy efficient morphology and behavior. This is expressed in considerable phenotypic variation in different sockeye salmon populations. Different populations are faced with varying difficulty of migration, depending on the distance of migration, the flow speed and turbulence within the river, the difficulty of passage, bear predation etc. This means that different selective pressure on energy efficiency is at work in different populations. Crossin et al (2004) showed using morphological analysis of body depth, body width and ratio of body width-to-depth in different populations that sockeye salmon in populations with more difficult journeys have shorter, more torpedo-like, fusiform body shape. This type of body shape is hydrodynamically more efficient as it is associated with lower hydrodynamic drag (Vogel, 1994). Also males in populations with difficult migrations grow smaller dorsal humps compared to the males with less demanding migrations (Hamon and Foote, 2005). As different populations do not cross-reproduce, these phenotypic differences are the result of local adaptation (Lin et al, 2008). Elongation of the snout and development of the hump involves the deposition of cartilage (Hendry and Berg, 1999), which is made up of protein. Muscle protein is utilized for these structural changes as fat reserves cannot be converted to protein. Fat reserves are expended on locomotion (Henry and Berg, 1999). In populations with more difficult migrations individuals it can be hypothesized that the males cannot "afford" a larger dorsal hump due to increased hydrodynamic drag (Crossin et al, 2004; Hinch et al, 2006).

The importance of hydrodynamic efficiency is also exemplified through comparisons of energetic demands of males and females and their morphology. Body constituent analyses for fish sampled before and after upriver migrations reveal that swimming activity depletes about half of the sockeye's total energy reserves (Brett, 1995). Roughly 55% of a female sockeye salmon's available energy is used for swimming activity, whereas 14% is used to

ripen gonads and 9% to reproduce (Hinch et al, 2006). Females allocate significantly more stored energy to gonad development than do males (14% vs. 2% respectively) (Brett, 1995). This means that females have to be more energetically efficient, because such a considerable part of their energetic resources goes to gonad development. Females indeed typically have more fusiform bodies than males and they do not grow dorsal humps. Electromyography (EMG) studies have shown that they also employ more efficient swimming patterns (Hinch et al, 2002). For example at reaches with river bank constrictions and complex river hydraulics where passage is most difficult, female sockeye salmon exhibited sustained and prolonged swimming speeds compared with males, which exhibited disproportionately high burst rates. At those reaches the energetic costs for male sockeye were an order of magnitude higher than that estimated for females (Standen et al, 2002).

Through these two examples, it is apparent that energetic efficiency is important to a varying degree for different individuals. Males in some populations can afford to grow larger humps than in other populations, and females who have a more constraining energetic budget because of the cost of gonad development, have to be more fusiform and hydrodynamically efficient than males.

This thesis is concerned with the question how exactly and to what extent does the dorsal hump affect the hydrodynamic drag of the male sockeye. Surprisingly this topic has never been investigated experimentally. The experimental biomechanical approach that will be pursued in this work will have a novel application. The following section will be an overview of another important aspect of sockeye biology, its mating and the role of the size of the dorsal hump in male reproductive success.

1.2. Reproduction and sexual selection in sockeye salmon

Quoting Theodosius Dobzhansky, “Nothing in biology makes sense except in the light of evolution“ (1973). If it is true that large dorsal humps are a hydrodynamic hindrance to the sockeye males as I hypothesize and intend to investigate experimentally in this thesis, then why have they evolved? Why can a trait that is disadvantageous persist throughout generations without being sieved out by natural selection? In essence this is the same question that Charles Darwin faced when he attempted to explain conspicuous traits in

males of many species (such as peacock tails, large antlers in deer, bright colors in cichlids etc.) through the theory of evolution by natural selection (Andersson, 1994). The problem lies in the fact that many such traits can be disadvantageous and harm the survival chances of those animals. For example, mating songs of male birds can attract predators; large antlers of deer are heavy and can get entangled in plant growth, etc. The paradox lies in the fact that these traits can increase mating success. In Darwin's (1859) words: ''A hornless stag or a spurless cock would have little chance of leaving offspring.''

This discrepancy led Darwin (1859) to coin the term sexual selection: ''Sexual selection... depends, not on a struggle for existence, but on a struggle between the males for possession of the females; the result is not death to the unsuccessful competitor, but few or no offspring.''. When natural and sexual selection for a trait oppose each other and that trait persists throughout generations, it can be inferred that the reproductive advantage males with the trait gain, is in the long run (evolutionarily) greater than that derived from a more perfect adaptation to its conditions of life (favored by natural selection) (Darwin, 1871). Of course many other traits, such as metabolic efficiency and pathogen resistance are favored by both natural and sexual selection (Andersson, 1994). In fact the modern view of sexual selection is that it is a subset of natural selection. The cause of natural selection is the external environment, physical or biological; the agents of sexual selection are a subset of that environment, sexual rivals and mates (Ghiselin, 1974). However when the evolutionary effect of sexual selection is very different from that of natural selection it is useful to view them as distinct, in the same way that Darwin did (Andersson, 1994).

Mating competition is the mechanism by which sexual selection acts upon a species. There are four main forms of competition over mates: contests, endurance rivalry, scrambles and mate choice (Andersson, 1994). Contests are displays or fights. They select for strength and weapons. Scrambles are about being the first to find the female. They favor well developed sensory and locomotory organs, but also good spatial memory. Endurance rivalry will favor males who remain longer at the breeding site and are thus able to fertilize more females. In mate choice the mate at stake influences whom they mate with. Mate choice selects for beautiful ornaments like the peacock tail and behavioral signals such as songs of birds. Quoting Darwin (1871) ''It appears that in a state of nature female birds, by having long selected the more attractive males, have added to their beauty.'' Mate choice form of sexual selection is especially important to this thesis as research on sockeye salmon mating

has shown that females select for males with larger hump size. The goal of this section is to describe the mating of sockeye salmon within the context of sexual selection. In fact all of the forms of mating competition described in the last paragraph also exist in sockeye salmon.

In the previous section the sockeye's migration upriver to the spawning grounds was described. During this journey sockeye salmon reach sexual maturity and sexual dimorphism is expressed through the growth of dorsal humps and kypes in males. Spawning takes place in population specific locations within 2-3 weeks (Quinn and Foote, 1994). Since the whole population of sockeye salmon does not enter the spawning ground at the same time, then the time of entry is associated with the scramble form of mating competition. A tagging study done on a creek population of salmon showed that sexual selection favored males who entered later relative to females, which may indicate that endurance rivalry (longevity on the spawning ground) is more important to mating success as the male to unspawned female ratios become skewed in the late phase of reproduction (Hamon and Foote, 2005). A mating study done on a close species pink salmon (*Onchorhynchus gorbuscha*), showed however that males who entered earlier were more successful in reproduction (Dickerson et al, 2005). As the scramble form of mating competition has not been extensively studied in sockeye salmon, it is impossible to make general conclusions about whether early arrival is important in mating success and as it is not directly connected to the subject of this thesis, I shall not further elaborate on it.

When the sockeye reach the spawning grounds a sequence of events unfolds. First the fish aggregate in shallow pools for a few days. Then the males scout the area and after that the females also explore, looking for suitable nesting sites. Once a suitable site is found, the female builds a nest (redd). The males then assemble around that female and an intense contest for her ensues.

Contests over females in sockeye salmon take place through several characteristic behaviors (Healey et al, 2003). Sockeye salmon show off through posture and lateral displays. Posture displays are performed by two competing males. They swim side by side with their bodies tilted up so that their noses protrude from the water. Often one male charges the other when he is in a favorable position to attack. The attacker accelerates towards the competitor and rams its side. They may then fight each other and bite using

their kypes (Healey et al, 2003). The kype is thus a weapon used against other males. In populations with intense mating competitions, individuals tend to have larger snouts, which is coherent with the theory of sexual selection (Hamon and Foote, 2005). Lateral displays are most commonly performed by the dominant male and are thus a form of turf defense. During lateral displays sockeye tenses its body and raises its dorsal fin in response to the approach of a contestant in an attempt to intimidate it. Sockeye can also perform digging behavior. During this it turns on its side and with powerful thrusts of its tail lifts substrate off the bottom, which is then carried downstream by water flow. Females use digging while building the redd and covering it after spawning, but the exact role of digging in males is not known. It may be a dominance behavior or a displacement behavior performed out of stress (Healey et al, 2003).

Through the outcomes of these interactions, a hierarchy of males is formed around the female fish, where the success of the male can be inferred from his proximity to the female (Quinn and Foote, 1994). Based on this the males are classified in the following manner: the closest male is called the consort. The consort has the role of the dominant male. Farther away are the satellite males, who are in active competition with the consort. Further still are the competitors, the males who are neither in consort or satellite position. The most unfortunate are alone, scouting the area looking for a ripe female to court.

When the time is right the consort moves into the redd beside the female and vibrates his body beside hers in an invitation to mate. The female can either accept him, in which case spawning takes place or chase him away and delay spawning. Observations have shown that when a female is surrounded by small males, she will delay spawning and thus exert control over whom she mates (Quinn and Foote, 1994). This is the mate choice form of sexual selection. Sockeye salmon are polygamous, so after the consort has spawned with one female he will typically move on to find another female to spawn with (Mehranvar et al, 2004). The male provides no non-genetic resources like parental care to the female or the young (Quinn and Foote, 1994).

Small males can sometimes use the sneak fertilization strategy. This means that they sneak behind the spawning pair and attempt to deposit some of their sperm onto the eggs (Hendry and Quinn, 1997; Mehranvar et al, 2004). However genetic investigations have shown that

the number of eggs conceived thus is small (Mehranvar et al, 2004). Males in the consort position fertilize most of the females' eggs (Mehranvar et al, 2004).

Quinn and Foote studied the effect of male morphology, specifically hump size, kype size and body length and reproductive success using morphometric measurements, tagging and observation (Quinn and Foote, 1994). The fish in this study were caught, tagged and their body depth, body length and kype length were measured. During the mating period observations were made through which it was determined how often the tagged male was a consort, satellite, competitor and alone. Using statistical analysis (multiple step regression) it was found that males with larger humps were the most successful and that hump size was statistically the best predictor of reproductive success. In other studies body length has been shown as a predictor of reproductive success (Foote and Larkin, 1988; Berejikian et al, 2000). Since body length and hump size are correlated in males(Quinn and Foote, 1994), then the fact that females are selecting males with larger humps may also contribute to the results where size has been shown to be selected for.

The last form of sexual selection is endurance rivalry. It has already been pointed out in the previous section that sockeye salmon have a limited energy budget of about 4 MJ/kg. Once this energy is exhausted they die. Success on the spawning grounds depends on energy, because all of the mating behaviors require energy. If the male has exhausted his energy resources on the migration he will fatigue and die earlier or he will not be able to afford the behaviors that would allow him to dominate over other males and become the consort. The energetic cost of different mating behaviors like posture and lateral displays have been studied using EMG telemetry by Healey et al (2003).

In the previous section the factors of natural selection selecting for energy efficiency in sockeye salmon were described. There is also a set of factors of natural selection on the spawning grounds. There are three main causes of mortality on the spawning ground. First they may die as a consequence of predation (mainly by brown bears (*Uranus arctos*) (Quinn and Kinnison, 1999). Second they may die as a result of stranding (this happens to fish whose body depth is too great for the spawning ground—they swim into water that is too shallow, get stuck and die of suffocation), this is true especially for shallow stream and creek spawning grounds (Lin et al, 2008). And finally they may die naturally of energy exhaustion as mentioned in the last paragraph. Thus the main factors of natural selection

impacting spawning salmon is predation and the spatial features of the spawning ground such as water depth.

A study of bear predation on sockeye salmon done by Quinn and Kinnison (1999) found by analyzing the corpses of sockeye salmon that bears preferred males over females and males with greater length and body depth were eaten more often. Thus in this case natural and sexual selection on hump size are of opposing nature. In some populations bears eat as many as 60% of sockeyes during their migration and spawning but other populations are not exposed to significant bear predation. It has been found that in populations with more accute bear predation males are smaller and exhibit less sexual dimorphism (have smaller dorsal humps) (Quinn and Kinnison, 1999; Hamon and Foote, 2005).

In populations for which spawning grounds are shallow, individuals have smaller body depth (Lin et al, 2008). In order to mate and leave progeny behind, individuals need to gain access to the spawning grounds. If they are unable to do so because of their morphology, they will not be able to pass on their genetic material and thus the future generation will have the traits of individuals who were able to navigate within the spawning grounds without stranding.

In conclusion: male sockeye salmon are subject to sexual selection during spawning and studies have shown that their mating success is correlated to their size and body depth (hump size). They are also exposed to natural selection on the spawning grounds stemming from bear predation and water depth of the spawning ground. It should be noted that the intensity of these factors of natural selection varies according to the population.

1.3. The problem statement of this thesis

If sexual selection favors larger hump size and natural selection favors hydrodynamic efficiency, then are these two in conflict? How does the dorsal hump affect the swimming performance of the sockeye?
In this thesis I turn to the biomechanical approach in order to answer these questions. Biomechanics is the application of quantitative engineering techniques to study how organisms perform mechanical functions and interact with their physical environment.

Biomechanicists view the organism as a machine consisting of physical parts that can be studied using engineering methods. This approach allows to elucidate the basic mechanical properties of organismal behavior and hence evaluate how structural characteristics affect performance and identify physical constraints on what animals can do. This information in turn can be used to assess the ecological function or niche of the organism or hypothesize about their adaptation and evolution (Koehl, 1996).

The engineering approach used in this thesis is computational fluid dynamics (CFD). Computational fluid dynamics is a branch of fluid mechanics that uses numerical methods and algorithms to simulate fluid flow on computers and thus allows to solve many fluid mechanics problems. Using CFD it is possible to simulate the flow around sockeye salmon models with different hump sizes and to obtain the fluid forces acting on the models and calculate their drag coefficients. By comparing the drag coefficients of the models it will become apparent if the hump size plays a role in hydrodynamic efficiency. From this it can be deduced whether the individuals are faced with a tradeoff between reproductive selection and energetic efficiency. Although some articles have hypothesized that the hump is indeed a hydrodynamic impediment, this question has never been investigated experimentally.

In order to explain the methodology of the experimental approach of this thesis and make conclusions, an overview of relevant fluid physics theory is required and it will be given in the following chapter. After that the chapter ''Fish hydrodynamics'' will apply these physical principles to fish locomotion and provide an overview of biomechanical studies of fish swimming.

2. PHYSICS OF FLUIDS

In order to understand the behavior, physiology and evolution of any animal you have to understand the physical environment that animal lives in. My object of interest in this thesis is essentially the physical interaction of a fish and its liquid environment. In order to answer the specific question of how morphology of the sockeye salmon impacts it's interaction with liquid environment, I first provide the necessary background in the physics of fluids.

In this chapter fundamental concepts pertaining to fluids and then moving fluids (fluid dynamics) will be described and finally the interactions of solids and flowing fluids will be taken into consideration. In the following chapter this knowledge will be applied to give a description of how fish interact with their environment and how these interactions have been studied by biologists using physical methods.

2.1. Fluid properties

2.1.1. What is a fluid?

So what is a fluid? For a start let's ask an easier question: What is the difference between a solid and a fluid? We know from our everyday experiences that solids are "hard" or not easily deformed, whereas fluids conform to forces that are exerted on them. If we look at the molecular structure of solids then we see that the "hardness" of solids comes from the fact that their molecules are densely spaced with large intermolecular attractive forces. This type of molecular structure "tries" to maintain its shape when a force acts on it. The molecules of fluids on the other hand have more free space between them and hence more freedom of movement. As a consequence of this they can be deformed, poured into containers or forced through tubes without much effort as our daily experience tells us.

In order to define the concept of a fluid more rigorously we need to introduce the concept of shearing stress. Shearing stress (τ) (force per unit area) is a force which is applied parallel to a surface divided by the area of that surface (IUPAC c). This is illustrated in

Figure 2.1. When we look at what happens to solids and fluids under shearing stress the picture is again very different. When solids are acted on by a shearing stress, they will initially deform, but at some point they will resist deformation. Fluids however will continuously deform when acted on by a shearing stress. This continuous deformation is called flowing. So fluid is defined to be a substance that deforms continuously when acted on by a shearing stress of any magnitude (Munson et al, 2006). There are some ambiguous materials such as tar, to which this definition doesn't easily apply, because they behave as solids when shearing stress is small, but when shearing stress exceeds some specific value, they flow. But certainly the substance this thesis is concerned with, liquid water, is a fluid and this definition suits it very well. In fact water is an almost perfect Newtonian fluid, which means that it shows a linear relationship between the applied shear stress and the resulting rate of deformation (Vogel, 1994; Munson et al, 2006).

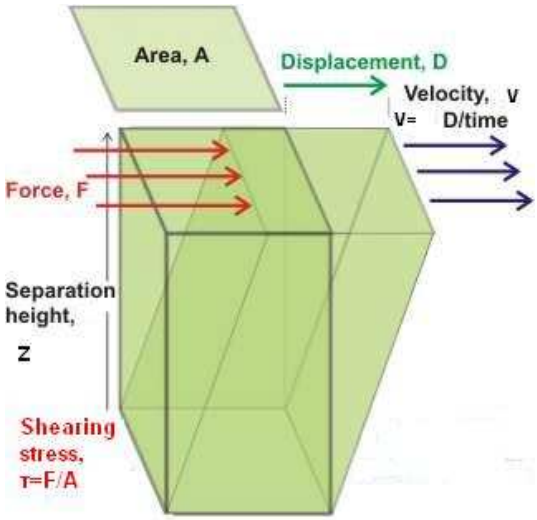

Figure 2.1. Shear stress applied to a volume of fluid (adapted after Chaplin).

Fluids can be classified into compressible and incompressible fluids based on how they react to pressure. Gases are compressible fluids since the volume of a given mass of gas changes easily with the change in pressure. Liquids are considered to be incompressible, since large pressure changes only lead to small changes in volumes. The physical substance this thesis deals with, liquid water, is an incompressible fluid.

In the beginning of this section fluids and solids were described in terms of their molecular structure. It is quite obvious that any matter is indeed a collection of interacting particles. However we have to forget about this when we want to study the behavior of fluids. Aside for the physical explanation of viscosity, viewing fluids as a collection of molecules only

complicates the matter. Because the number of particles involved is immense, we cannot describe the behavior of a fluid through the motions of individual particles. This is because when a large number of particles interact, it becomes quite impossible to calculate and predict the resulting motion by taking into account the individual motions of the particles. For this reason fluids are treated as a continuum. They are assumed to be nonparticulate and infinitely divisible. This means that instead of the motion and properties of individual particles the average over a small volume containing a large number of particles is considered. In short, instead of considering a point in a fluid a small volume around that point is considered. This is why in a continuum physical properties such as velocity, density, temperature, stress etc. are said to vary continuously throughout the fluid.

2.1.2. Density

The density of a fluid (ρ) is defined as its mass per unit volume:

$$\rho = \frac{m}{V}\ , \qquad (2.1.)$$

where ρ (kg/m^3) is density, m (kg) is mass and V (m^3) is volume.
Density is involved in such fluid properties as kinematic viscosity and Reynolds numbers, these properties shall be discussed below.

2.1.3. Viscosity

In order to define viscosity we have to return to shear stress. Consider two negligibly thick parallel flat plates of the same shape and area (this area is big, so that edge effects on the fluid may be ignored) separated by a fluid filled space. One plate is held stationary and the other is pushed with a force F parallel to its plane. In other words a shear stress is applied to that plate. Because of the definition of a fluid that was established in the last section the fluid between the two plates then undergoes shear flow. For straight, parallel and uniform flow shear stress is proportional to the rate of shear deformation (and also to the velocity gradient) in the direction perpendicular to the layers. Viscosity (also called dynamic viscosity) is then the proportionality factor (IUPAC a, d). In equations this can be expressed as:

$$\tau = \frac{F}{A} = \mu \frac{\partial u}{\partial z} = \mu \frac{\partial u}{\partial z} \tag{2.2.}$$

and

$$\mu = \tau \left(\frac{\partial u}{\partial z} \right)^{-1}, \tag{2.3.}$$

where τ (N/m^2) is shearing stress, A (m^2) is area, u (m/s) is velocity, z (m) is the third Cartesian dimension normal to the surface A and μ (Ns/m^2) is dynamic viscosity.

In the previous section it was mentioned that in defining viscosity, we have to return to thinking about the molecular structure of the fluid (indeed further on when viscous effects will be taken into account in the formation of a boundary layer around an immersed body, this view of the fluid will once again be adopted). We can then view the fluid as consisting of layers of fluid or little tubes of fluid moving side by side. In any flow these layers of fluid move at different velocities and fluid's viscosity arises from the shear stress between the layers that oppose the applied force. Viscosity is thus the property that describes the fluid's internal resistance to flow. It can be described as the internal "friction" of the fluid.

Another important quantity is the kinematic viscosity of the fluid. Many aspects of flow, such as how likely it is to break into vortices, how steep the velocity gradients in the flow will be, depend on it (Vogel, 1994). It is simply the dynamic viscosity divided by the density of the fluid (IUPAC b):

$$\upsilon = \frac{\mu}{\rho}, \tag{2.4.}$$

where υ (m^2/s) is kinematic viscosity.

Kinematic viscosity is actually a sort of measure between the viscous forces and inertial forces in the fluid, with the latter being characterized by density. Inertia is the resistance of an object to a change in its motion. Inertial forces are then forces that resist changes in motion of an object. From this we see that viscous forces and inertial forces in moving fluids are of opposing nature. The character of flow depends on which sort of forces dominate. The following paragraph will introduce the concept of Reynolds number, which characterizes the relative importance of inertial and viscous effects in a flow.

2.1.4. Reynolds number

In 1883 Osborne Reynolds, a British engineer was conducting experiments with fluid flows. He introduced a dye stream into a pipe of flowing fluid as an indicator of whether the flow was laminar or turbulent. If the streak remained straight, then the flow would be recognized as laminar and if it dissipated it would be classified as turbulent.

Laminar flow and turbulent flows have opposite character. Laminar flow is a "smooth" flow. The fluid flows in parallel layers with no disruption between the layers. That is why the dye streak in laminar flow remains straight—it is one of the layers of flow, it does not mix with the others. Turbulent flow on the other hand is chaotic. Properties of flow like velocity and pressure gradients change in a stochastic way. Vortices and eddies are formed. The dye streak in turbulent flow dissipates in a stochastic and unpredictable way.

In Reynolds' experiment as in most other fluid flow problems involving solids and fluids, there were four parameters that could be varied: characteristic length (in this case it was the pipe's diameter, in the case of immersed bodies in fluids it would be some measure of that body), free-stream velocity and fluid properties of density and viscosity. By varying these parameters Reynolds discovered that flow could be made to shift from laminar to turbulent in several ways: by increasing speed; by increasing the diameter of the pipe; by increasing the density of the liquid; or by decreasing the liquid's viscosity. All of the changes had the same amount of impact on the character of flow and they were effective in combination as well as individually. Reynolds discovered that when the value of a certain combination of these variables exceeded 2000 the flow became turbulent. This combination is what is called Reynolds number (*Re*):

$$\mathrm{Re} = \frac{\rho U l}{\mu} = \frac{U l}{\nu}, \qquad (2.5.)$$

where l (m) is characteristic length and U (m/s) is free stream velocity.

Reynolds number also arises mathematically by applying dimensional analysis and Buckingham's Pi theorem to these variables. Reynolds number is the most famous dimensionless parameter in fluid mechanics. It gives a rough idea of how the flow

behaves—in the same *Re* the flow around geometrically similar objects behaves in much the same way. In Figure 2.2. a flow around a circular cylinder at different *Re* is shown. The transition from laminar to transitional and to turbulent flow with the increase in *Re* is observable. At *Re*=0.2 the flow around the cylinder is laminar and fully attached to the cylinder. At *Re*=12 the cylinder bears a pair of attached vortices. At *Re*=120 these vortices alternately detach from the cylinder and flow downstream, each rotating in an opposite direction than the one before it. This pattern is called the Von Karman trail. At *Re*=30,000 the fluid directly surrounding the cylinder (boundary layer) is in the laminar flow regime, but the wake of the fluid is turbulent. At *Re*=500,000 the flow is fully turbulent, chaotic.

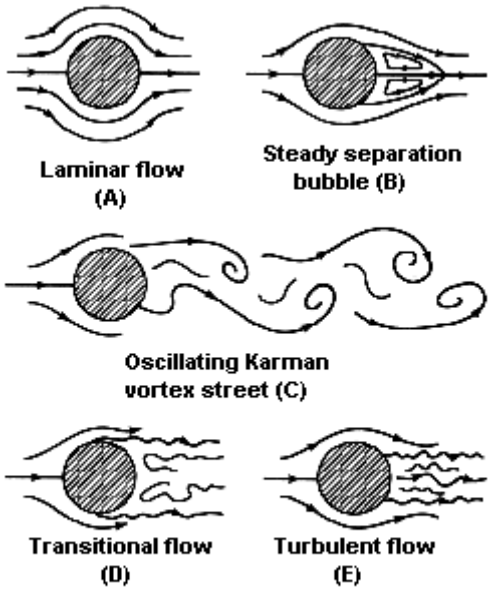

Figure 2.2. Flow around a circular cylinder at different Reynolds numbers. (A) *Re*=0.2; (B) *Re*=12; (C) *Re*=120; (D) *Re*=30,000; (E) *Re*=500,000 (after Vogel, 1994 and Munson et al, 2006).

Reynolds numbers can also be derived through the analysis of fluid forces. In the previous section we saw that there are two types of forces affecting the behavior of the fluid: viscous forces and inertial forces. Inertial forces are attributable to the momentum of moving fluid. Inertial forces for fluids are derived through Newton's second law:

$$F_I = \rho A U^2 \quad , \qquad (2.6.)$$

where F_I (N) represents inertial forces and A is the area through which the fluid is flowing. Viscous forces are defined modifying equation 2.2:

$$F_V = \frac{\mu A U}{l}, \tag{2.7.}$$

where F_V (N) represents viscous forces and A (m^2) the area to which the force is applied. By dividing these two forces we once again obtain the Reynolds number:

$$\frac{F_V}{F_I} = \frac{\rho U l}{\mu}, \tag{2.8.}$$

So it is apparent that the Reynolds number is a measure of the ratio of the inertial forces to viscous forces in the fluid. This is why the Reynolds number indicates the character of flow. Equality of the Reynolds number for two situations guarantees that the physical character of the flows will be the same. This doesn't mean that the forces are the same, but the patterns of flow are of similar character. This property of *Re* makes it a useful tool for the classification of flows.

Organism	**Reynolds Number**
A large whale swimming at 10 m/s	$3*10^9$
A tuna swimming at the same speed	$3*10^8$
A duck flying at 20 m/s	$3*10^6$
A dragonfly going 7 m/s	$3*10^5$
A copepod in a speed burst of 0.2 m/s	300
Flapping wings of the smallest flying insect	30
An invertebrate larva, 0.3 mm long, at 1 mm/s	0.3
A seaurchin sperm swimming at 0.2 mm/s	0.03
A bacterium swimming at 0.01 mm/s	10^{-6}

Table 2.1. Reynolds numbers for self-propelled organisms (after Vogel, 1994).

Re is also important to biologists, because organisms living at similar *Re* have similar functional adaptations, because they deal with a similar kind of flow. *Re* show, whether the predominant forces that an animal faces are viscous or inertial. Although a whale and a bacterium are both swimming essentially in the same water, because of their differences in size and hence Re, the forces they encounter are very different. The whale feels almost no viscous forces, but to the bacterium water is a like thick sticky jam, because of the

dominance of viscous forces at low Re (Vogel, 1994). There are particular propulsive mechanisms and morphologies that are suited for different Re. A spermatozoon at low Re cannot swim using the same mechanisms as a fish at high Re, because fish propulsion relies on inertial forces, which are almost non-existent at low Re. Hence a spermatazoa uses a flagellum, which is much more effective in fluids dominated by viscous forces. Below a table of different animals and their characteristic Re is given for illustration.

Having supplied these basic definitions that apply to both static and moving fluids, the next section will present the fundamental principles governing the behavior of fluid flows.

2.2. Fluid dynamics

Any fluid flow is governed by three fundamental principles: conservation of mass, Newton's second law and conservation of energy. These principles are expressed mathematically through the continuity equation, momentum equation and energy equation. These equations are important in that they are necessary to model fluid flow. In computational fluid dynamics these equations are discretized and solved numerically. In this section a description of these equations will be given.

2.2.1. Conservation of mass

Conservation of mass principle states, that the amount of mass in a system is constant. This means that mass cannot be created or destroyed and that the rate at which mass enters a system is equal to the rate at which mass leaves the system.
The mathematical expression for this principle is called the continuity equation. The differential form of this is:

$$\frac{\partial \rho}{\partial t} + \nabla \cdot (\rho u) = 0, \qquad (2.9.)$$

where t (s) is time.
If density is constant as it is for incompressible fluids such as water, then this equation takes the simpler form:

$$\nabla \cdot u = 0. \qquad (2.10.)$$

This equation means that in incompressible fluids the divergence of the velocity field is zero everywhere.

2.2.2. Newton's second law, Navier-Stokes equations

Newton's second law of motion states that the net force acting on a body is equal to the particle's mass times the acceleration:

$$F = ma, \qquad (2.11.)$$

where a (m/s^2) is acceleration.

In fluids this equation will hold for any fluid particle. However fluids are viewed as a continuum, not a collection of particles as was discussed above. Navier-Stokes equation is the application of Newton's second law to a flowing continuum. It is a non-linear partial differential equation:

$$\rho\left[\frac{\partial u}{\partial t} + u \cdot \nabla u\right] = \nabla u \cdot \sigma + f, \qquad (2.12.)$$

where σ (N/m^2) is normal stress and f (N/m^3) is body force acting on the fluid.

For viscous Newtonian fluids Navier-Stokes equation can be translated into the following equation:

$$\rho\left[\frac{\partial u}{\partial t} + u \cdot \nabla u\right] = -\nabla p + \mu \nabla^2 u. \qquad (2.13.)$$

The left hand side of the Navier-Stokes equations is density times acceleration. The acceleration is written as the sum of two effects. The local acceleration $\frac{\partial u}{\partial t}$ is a result of unsteadiness of the flow (Homsy et al, 2000). The convective acceleration $u \cdot \nabla u$ is a result of the spatial variation of the velocity field (Homsy et al, 2000).

The right hand side of the Navier-Stokes equations is the net force per unit volume acting on the fluid (Munson et al, 2006). For the general form of Navier-Stokes these forces are the result of various normal stresses and shear stresses. For Newtonian fluids these are pressure and viscous forces.

Solution of Navier-Stokes equation is a velocity field, which describes the velocity of the fluid at a given point in space and time. Through the velocity field other quantities such as flow rate and drag or lift forces may be found. This is why Navier-Stokes equations are important in fluid mechanics. Their solutions describe a wide variety of fluid mechanics phenomena.

2.2.3. Conservation of energy

Much like the principle of conservation of mass, the principle of conservation of energy states that the total amount of energy in an isolated system remains constant. Energy cannot be created or destroyed.

The mathematical expression of this statement is called the energy equation. Its differential form is:

$$\rho\left(\frac{\partial \varepsilon}{\partial t} + u \cdot \nabla \varepsilon\right) - \nabla \cdot (K_H \nabla T) + p \nabla \cdot u = 0, \qquad (2.14.)$$

where ε (J) is thermodynamic internal energy, K_H is thermal conductivity of the fluid (W m^{-1} K^{-1}), p (N/m^2) is pressure and T (K) is temperature.

The energy equation is important in such phenomena as heat transfer. In very precise calculations of fluid flow the energy equation is taken into account, since heat can also influence fluid movement. However in this investigation heat phenomena are not accounted for since their effect is negligible. The energy equation is given here for completeness, but will not be used.

2.3. Immersed bodies

Having defined the basic properties of fluids and the governing equations of fluid dynamics, we now come to the part that was already briefly touched upon when talking about Reynolds numbers. This section will consider what happens to bodies that are immersed in fluids and attempt to answer the question, how do solids and fluids interact.

2.3.1. Boundary layer

Fluid flow is influenced by the presence of solid boundaries. Since fluid cannot cross a solid boundary, it must therefore go around the body. The fluid sticks to the solid boundary due to viscous forces (this is called the no-slip condition). This means that the slender fluid layer touching the boundary has the velocity equal to the velocity of that boundary. The fluid adjacent to the wall has a velocity gradient with the velocity of the fluid layers increasing with the distance from the boundary. The thin layer around the immersed body that displays this velocity gradient is called the boundary layer. The boundary layer is illustrated in Figure 2.3.

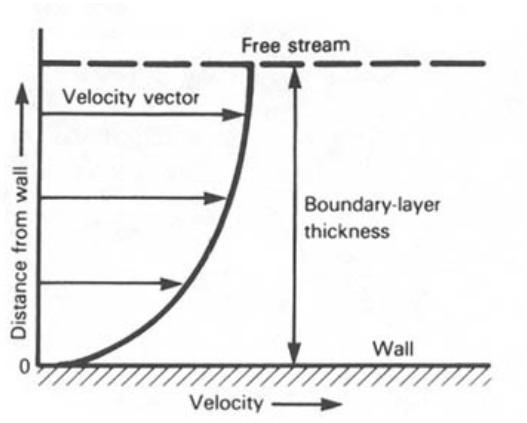

Figure 2.3. Boundary layer of a solid within a fluid. The no-slip condition and velocity gradient of the fluid is shown (from Roland, 1985).

The distance over which the viscous forces have an effect is known as the boundary layer thickness. The boundary layer thickness is a function of Reynolds number because it depends on the ratio of inertial forces and viscous forces in the flow. As Reynolds number increases, boundary layer thickness decreases. The nature of boundary layer also depends on the texture of the surface. Boundary layer effects are the cause for viscous drag, which shall be described in the following sections.

2.3.2. Pressure

To introduce the concept of pressure in fluid flows we must first discuss the concept of streamlines. Very simply streamlines are like paths through which flowing fluid particles travel and which they never cross. The velocity vectors of these particles are always tangent to that path. This means that the local direction of fluid movement is everywhere tangential to streamlines. Streamlines are illustrated in Figure 2.4.

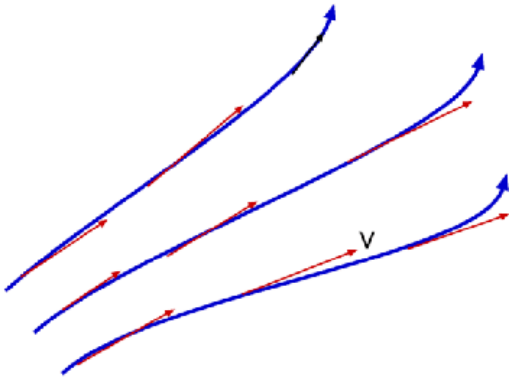

Figure 2.4. Streamlines of a fluid (blue lines) in a velocity field (velocity vectors are red arrows) (from VisualizationWiki).

Newton's second law of motion can be integrated along the normal to a stream line, if the flow is assumed to be inviscid (lacking viscosity) steady and incompressible. Through this a famous equation called the Bernoulli equation is obtained:

$$p + \frac{\rho U^2}{2} + \gamma z = \text{constant along streamline,} \qquad (2.15.)$$

where p is static pressure (N/m^2), γ (N/m^3) is specific weight and z (m) is depth.

Each term in the Bernoulli equation represents a form of pressure. The first term, p, is static pressure. Its value is measured by moving along with the fluid (thus being static relative to the moving fluid). The second term is called dynamic pressure. Dynamic pressure is the pressure that can be measured when a moving fluid is suddenly brought to a halt by a solid boundary-- it is thus related to the kinetic energy of the fluid. The third term is called

hydrostatic pressure. It is the pressure on the fluid caused by the height of the fluid above it. Total pressure of the fluid is the sum of static pressure, dynamic pressure, and hydrostatic pressure.

Pressure plays a role in the phenomenon of flow separation and drag, which will be discussed below.

2.3.3. Drag

Drag is a measure of how much the fluid resists the movement of an immersed body. The body in turn removes momentum from the flowing fluid. Drag of a body is the rate at which this momentum is removed (Vogel, 1994).

The formula for drag force is obtained through dimensional analysis. The variables upon which the drag of an object in fluid depends are the size of the object, it's speed relative to the fluid, and the viscosity and density of the fluid (Vogel, 1994). Buckingham's Pi Theorem predicts that the formula will be the product of two terms—one of them with dimensions of force and the other dimensionless. The force term is the dynamic pressure times the area of the object. The dimensionless term is an exponent function of Reynolds numbers:

$$C_d = (\mathrm{Re})^a = f(\mathrm{Re}) \tag{2.16.}$$

and

$$D = (\frac{1}{2}\rho A U^2)(\mathrm{Re})^a, \tag{2.17.}$$

where D is drag force (N) and C_d is drag coefficient (dimensionless).

While the first term of drag is independent of the body's shape, the drag coefficient accounts for the effect of shape on drag force. The drag coefficient is not a constant. There is no formula for the attainment of drag coefficient for an object with given dimensions, so it has to be experimentally measured for a given Re. So it essentially represents an experimental ratio of measured drag force D to the dynamic pressure times the reference area of the object:

$$C_d = \frac{2D}{\rho A U^2} \tag{2.18.}$$

and

$$D = \frac{1}{2} C_d \rho A U^2 . \tag{2.19.}$$

This formula gives a way to convert the drag coefficient into drag force and vice-versa. It is a simplification because instead of having to find out how drag varies with speed, size, viscosity and density, only the information on how the drag coefficient varies with Reynolds numbers is needed. Drag force depends most heavily on velocity.

The *A* term in the formula for drag is called the reference area. It is a rough characteristic of the shape of the organism. There are different reference areas in use for different objects in flow. The most common ones are: frontal area, profile area, total area and volume to the two-thirds power (Vogel, 1994). Each of these reference areas is used in particular situations. The reference area relevant to this thesis is the total area, because it is commonly used for streamlined bodies. It is the area of body surface interacting with the fluid. Because the drag coefficient depends on the chosen reference area, the chosen reference area has to be indicated along with the drag coefficient data, otherwise this data can be misleading (Vogel, 1994).

2.3.4. Flow separation

Flow separation is basically the flow and boundary layer breaking away from the surface of the body. It is induced pressure fields where pressure increases in the streamwise direction. It occurs when the flow momentum near the surface insufficient to overcome the increasing pressure. The point at which this occurs is called the separation point. At the separation point the fluid becomes detached from the body (stops following the surface of the body) and takes the form of vortices that flow downstream.

Flow separation results in a drastic increase in drag because it results in fluid energy being dissipated in the rear through vortices and turbulence. This means that the dynamic pressure on the front of the body is not counteracted by an equal and opposite pressure on the rear. This disbalance in pressures is felt as drag on the body.

This section concludes the review of basic fluid physics. In the next section these physical principles will be applied in the study of fish hydrodynamics.

3. FISH HYDRODYNAMICS

This chapter will apply the physical principles described in the previous chapter to fish locomotion.

The first section of this chapter will give a basic overview of fish hydrodynamics. The second section will describe the different methods used by biologist in the study of hydrodynamics of fish and their contribution to our understanding of fish biology through an overview of representative articles. The final section will demonstrate the contribution and novelty of this thesis in light of the studies and methods described in the second section.

3.1. Forces acting on a fish in locomotion

The physical properties of water that play an important role in the life, locomotion and evolution of fish are its high density, incompressibility and viscosity. Mainly because of these properties of water compared to air, the magnitudes of forces that fish face are very different to those faced by animals living in air. Figure 3.1. is a schematic overview of forces acting on a swimming fish.

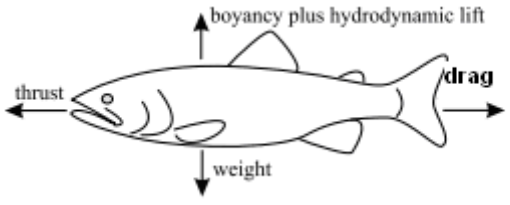

Figure 3.1. Forces acting on a swimming fish (from Lane et al, 1998).

The density of water is about 800 times that of air. Fish body density is close to the density of water, so the net weight of a fish in water is small compared to that on land. This means that the effect of gravitational force acting on the fish is relaxed.

Since water is an incompressible fluid, the movement of fish in the water sets it in motion and vice versa (Lane et al, 1998). So fish swimming works by momentum transfer from the movements of fishes body to the fluid. The momentum transferred can be thought of as the mass of water that is accelerated by the fishes body to an average given velocity. The rate

at which the fish transfers momentum to the water determines the amount of thrust that it generates (Biewener, 2003). This thrust can be quantified as:

$$T = \frac{mu}{t}, \tag{3.1.}$$

where T (N) is thrust.

Work that has to be done by a fish to go a certain distance with a constant thrust is:

$$W = T \cdot d, \tag{3.2.}$$

where W (J) is work and d (m) is distance.

Power is the rate at which work is performed by a fish swimming at a given thrust is given by the following equation:

$$P = \frac{W}{t} = T \cdot u, \tag{3.3.}$$

where P (W) is power.

Fluid in turn resists and pushes back on the fishes body opposing thrust. The fluid's resistive effect on the fish is called drag. In order for the fish to move the thrust force must be equal to or overcome the drag force.

Drag was already discussed in previous chapter. It depends among other things on the viscosity of the fluid. Mechanical power requirements of movement is much higher for fish than birds, because of higher viscosity of water. This is why drag reducing mechanisms are especially important for fish—they can potentially lose much more energy to drag than birds for a given speed.

Drag on the fish has three components: viscous drag, which arises from boundary layer effects or in other words interactions between the surface of the fish and water; body form drag (also called pressure drag) which depends heavily on the shape of the body as it results from the distortion of flow by the body and; induced drag, which comes from the motion of moving caudal and pectoral fins redirecting the flow around them (Lane et al, 1998). A set of adaptations exist in fish to minimize each of these components of drag and thus minimize energy expenditure during swimming.

Viscous drag is important at low Reynolds numbers, but the higher the Re the less influence it has on the total drag of the organism. The main mechanisms for viscous drag reduction in fish are scales and surface additives (polymers, surfactants, bubbles). Fish slime is a very effective drag reduction mechanism, it can reduce viscous drag up to 50%

(Bushnell, 1991; Sagnes et al, 2000). The morphological features of some fish such as tubercules, folds and spinelets also serve a drag reducing purpose. They do so by establishing turbulent flow in some regions of the fish's body, which locally thickens the boundary layer along the flow direction. Skin drag decreases with boundary layer increase (Bushnell, 1991).

Form drag in turn is relatively unimportant at low Re, but becomes more and more prominent with the increase in Re. The fundamental problem of form drag reduction is to avoid flow separation, because any object from which flow separates will experience high levels of drag because of the energy lost in the rear (see the previous chapter for the section ''Flow separation''). Typically the forward portion of the body is a region of falling pressure, whereas the rear portion is subject to increasing pressure. Because of this the rear body is prone to large scale flow separation (Bushnell, 1991). This means that for fish the design of the rear body is important in mitigating form drag through avoiding flow separation. This can be achieved through streamlining of the body. A streamlined object has a rounded front and from the midsection the body gradually curves back to a tapered rear section. The fluid flowing over a streamlined body gradually decelerates in the rear and very little or no separation occurs (Vogel, 1994). In the case of sockeye salmon the dorsal humps of males are expected to have an impact on the body form drag of the fish because the bigger the hump the less streamlined the body shape is.

Induced drag results from the vortices shed by moving fins. It can be reduced through the increase in the aspect ratio of the fin (length of the fin divided by it's thickness), because the thinner the fin, the smaller the vortices breaking away from it's tip. This approach is limited by the concern for the structural strength and durability of fins, but is employed in fish to the greatest extent possible (Bushnell, 1991). Induced drag doesn't play a role in the subject of this thesis, so I shall not elaborate on it further.

Much in the same way that drag results from the uneven distribution of fluid pressure on the front and the rear of the body, lift is the result of uneven pressure disribution on the belly and the dorsal side (back) of the fish. When the pressure on the back of the fish is lower than the pressure on the belly of the fish, this results in positive lift force, which pushes the body in direction normal to the fluid flow.

Having described the forces acting on a swimming fish, a more specific overview of biomechanical studies of fish swimming will be provided in the next section.

3.2. Biomechanics approach to fish swimming studies

This section provides reviews recent literature around three recognised approaches to the study of fish hydrodynamics. These methods are DPIV, CFD and real-life drag measurements. Through this review, the author hopes to illustrate the efficacy of a biomechanics approach to this problem.

3.2.1. Real-life drag measurements

In the article ''Shifts in drag and swimming potential during grayling ontogenesis'' (Sagnes et al, 2000) the drag coefficient of the five life-stages of grayling (*Thymallus thymallus*) was investigated. This was done by measuring the drag forces on the clay models of younger stages and the freshly killed/formalin prepared fish for the older stage in a flow tank. The measurements were done on rigid bodies. Figure 3.2. illustrates the experimental set up.

During its ontogenesis grayling undergoes significant morphological changes. The article found that drag coefficient decreased with each successive morphotype and as their muscle mass grew so did the swimming potential.

The method used in this article is consistent with that in many other articles. Biologists have studied the drag of organisms in air and in water to answer questions about their way of life, adaptation to their environment or approximate their energetic requirements. This has been done using wind and water tunnels to measure the forces acting on the organisms with a loadcell as it was done in this article (Pennycuick et al, 1988; Lovvorn et al., 1991; Lovvorn et al, 2001; Shelley&Vogel, 2000; Puijalon et al, 2005) , using video techniques to measure the deceleration of gliding animals in water (Bilo, Nachtigall, 1980; Stelle et al, 2000), using modelling techniques (Miller et al., 2004) or using computational fluid dynamics (Borazjani and Sotiropoulos, 2008, 2009).

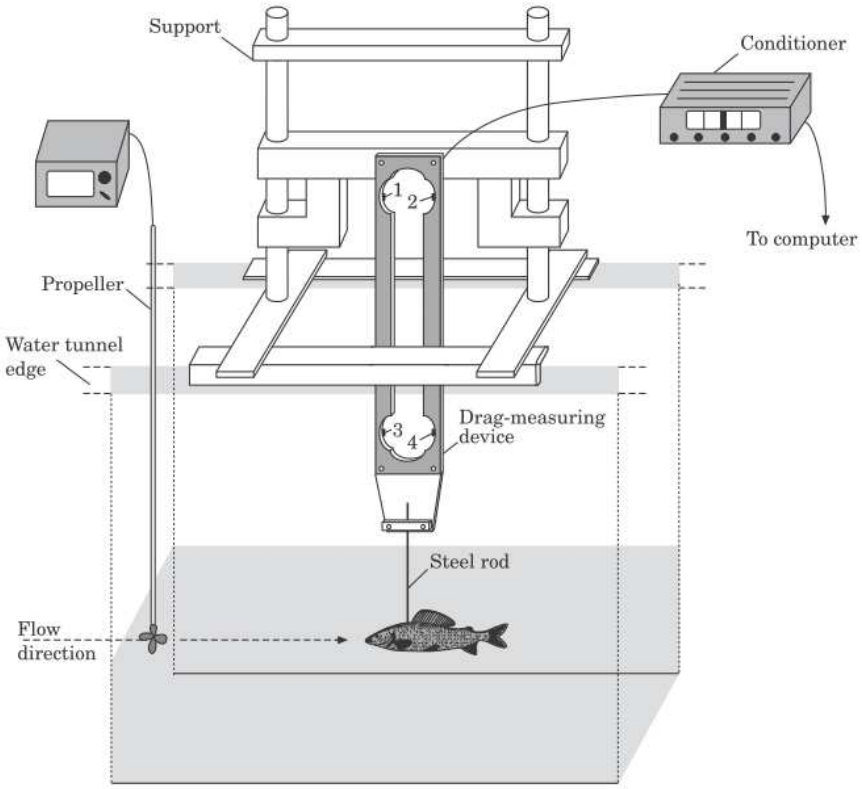

Figure 3.2. Experimental device for the measurement of rigid fish body drag in a water tunnel (from Sagnes et al, 2000). Numbers 1-4 represent strain gauges of the measuring device.

With the exception of the relatively recent computational fluid dynamics approach, all of these techniques measure the drag of rigid bodies. Measurements of rigid body drag suffer from many limitations. In fish locomotion either the whole body or certain structures participate in the production of thrusts and this significantly alters in shape. Rigid body drag doesn't provide a realistic picture of the type of drag forces a swimming fish encounters, except for fish who swim with relatively rigid bodies using only their pectoral fins. Rigid body drag also cannot be used to make accurate predictions of fish power consumption and thus energetics. The energy needed to produce enough thrust to overcome rigid body drag doesn't take into the account that the fish's body shape and thus drag changes while it produces thrust.

This limits the comparability of rigid body drag measurement results, especially when the fish who are being compared employ different swimming modes. The results of this article

thus have little comparative power, because the different morphotypes of grayling employ different modes of swimming. The younger stages employ the anguilliform swimming mode (almost the entire body undergoes undulations) and older stages shift to the carangiform mode (undulations are limited to the caudal region of the body) (Sagnes et al, 2000). These modes of swimming are cardinally different and because of that, the relationship between the measured rigid body drag and the actual drag that a swimming grayling encounters is different for each of the morphotypes. This means that a morphotype that has a higher rigid body drag than another morphotype may still encounter a lower drag force while swimming, because it employs a more efficient swimming mode. This in turn means that the conclusions made from the comparison of the rigid body drag of different models without taking into account the swimming modes that they employ are unreliable and do not form a realistic illustration of real world dynamics.

Nevertheless this article illustrates the methods traditionally used by biologists to study hydrodynamics of aquatic organisms. The advent of new technologically advanced methods such as digital particle image velocimetry (DPIV) and computational fluid dynamics have brought a more detailed knowledge of fish swimming biomechanics.

3.2.2. How do swimming modes and Strouhal numbers of the caudal fin impact the drag and thrust of fish?

In the articles ''Numerical investigations into hydrodynamics of carangiform swimming'' (Borazjani and Sotiropoulos, 2008) and ''Numerical investigations into hydrodynamics of anguilliform swimming'' (Borazjani and Sotiropoulos, 2009) accurate computer models (obtained from computer tomography scans of real fish) of a mackerel (*Scomber spp.*) and a lamprey *(Petromyzon spp.)* are simulated as flexible moving bodies using computational fluid dynamics. The motion prescribed to them is biologically accurate, obtained from mathematical investigations of fish kinematics (where fish motion was translated into Fourier series). The simulations are performed in inertial (high *Re*), transitional and inviscid flow (infinite *Re*).

Mackerel and lamprey employ radically different swimming modes. Mackerel is a carangiform swimmer which means that it produces thrust with the caudal portion of it's body. The lamprey is an anguilliform swimmer that employs whole body undulations for propulsion. The Strouhal number was systematically varied for both of these forms of

propulsion. Strouhal number is a dimensionless parameter describing oscillating flow. It is defined as:

$$St = \frac{fA}{U}, \qquad (3.4.)$$

where U (m/s) is the steady swimming speed of the fish, A (m) is the maximum lateral excursion of the tail over a cycle.

In this study the relationships between Strouhal numbers, Reynolds numbers and thrust and drag forces on both fishes were investigated. Figure 3.3 summarizes the important results considering the relationship of *St* and thrust and drag forces. Their results showed that there is a critical *St* number for which thrust becomes equal to drag and exceeds it (the fish propels itself forward). It was also shown that critical *St* depends on Re. Further increase in *St* beyond the critical *St* number leads to more intense thrust force production. For values below the critical *St* however body undulations actually increase drag forces acting on the swimmer.

It is also apparent from figure 3.4. that the amplitude of the fluctuations of axial force coefficient is very different for anguilliform and carangiform swimmer. Through the manipulation of this data Borazjani and Sotiropoulos showed that anguilliform swimmers are smoother swimmers. They were also able to show that carangiform mode of swimming is most affective at high *Re* flow and anguilliform mode of swimming at low *Re*. This is of great biological significance, as the mackerel lives at high Re whereas the lamprey at low *Re*. This is thus evidence of biological adaptation.

This article also investigated the connection between body form drag and *St*. The results showed that initially for small *St* the form drag of the fish increases, but later falls and asymptotes toward zero. It was found that whether drag decreases or increases for a give *St* depends on the ratio of the undulatory wave phase velocity V to the swimming speed U. This is because of the phenomenon of flow separation. It was mentioned above how the fundamental problem of form drag reduction is avoiding flow separation. In this article it was shown that when $V<U$ (for small *St*) the flow separates, but when $V>U$ separation is eliminated. At the *St* where flow separates the fish experiences considerable drag increase, but for *St* where the $V>U$ condition is met the body form drag of a moving fish is actually lower than that of the rigid fish. This result points to how fish locomotion has evolved to be very efficient. Flow separation phenomena is illustrated in Figure 3.4.

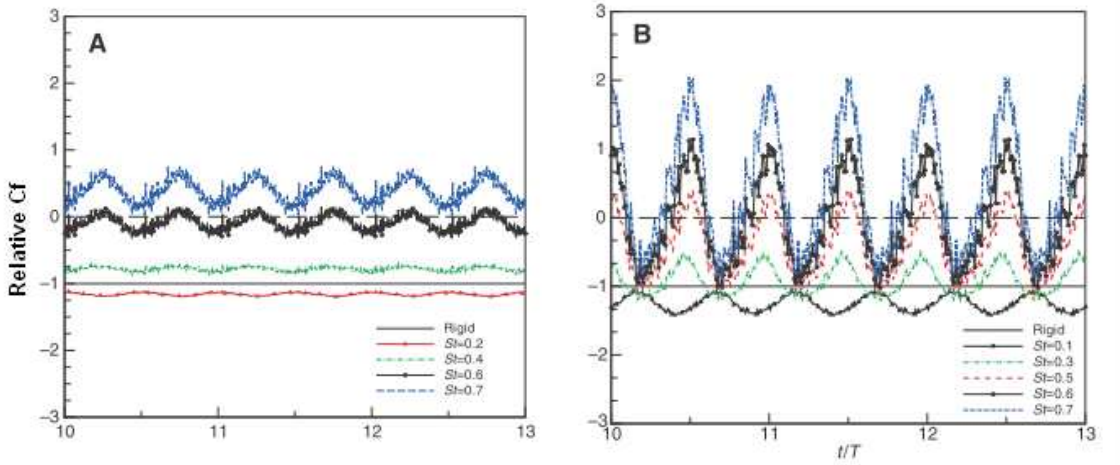

Figure 3.3. Time history of the axial force coefficient C_f normalized by rigid body drag for different *St* at *Re*=4000. A) Virtual lamprey compared to B) virtual mackerel. Positive values indicate that the force is of thrust type, negative values that the force is of drag type (from Borazjani and Sotiropoulos, 2009).

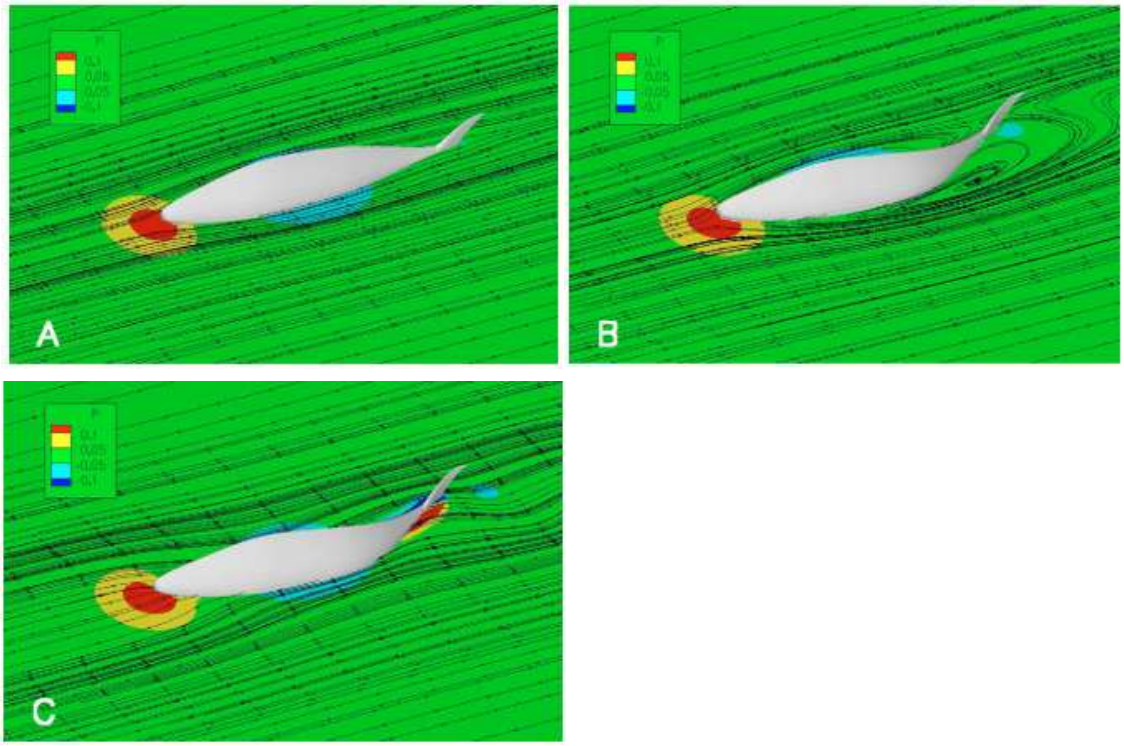

Figure 3.4. Pressure contours for the CFD simulations of the mackerel at *Re*=300. A) Rigid body (*St*=0), flow doesn't separate. B) *St*=0.1, U/V=2.11, flow separates. C) *St*=0.3, U/V=0.7, flow doesn't separte (after Borazjani and Sotiropoulos, 2008).

I chose to review these studies in these section because they represent the current state of the art in biological CFD. Other CFD studies on fish swimming include Barrett et al (1999), Wolfgang et al (1999) and Zhu et al (2002). CFD has also been used to study the locomotion of tadpoles (Liu et al, 1996, 1997) and insect flight (Aono et al, 2008).

3.2.3. How does the position and orientation of the pectoral fin impact the manoeuvring of the fish?

This section is based on the research paper "Wake dynamics and locomotor function in fishes: interpreting evolutionary patterns in pectoral fin design" (Drucker and Lauder, 2002). In this article digital particle image velocimetry (DPIV) is used to provide insights into how the evolution of ray-finned fishes (*Actinopterygii*) has affected the function of the pectoral fin. DPIV is quantitative imaging technique, which uses a laser light sheet to illuminate small reflective particles seeded into the water in a flow tank. Images of these laser planes are recorded using a high-speed video camera and the motion of reflective particles can then be tracked and quantified using computer software. The obtained data allows detailed flow visualization and physical analysis of fluid velocity. DPIV was originally developed for the analysis of non-biological flow, but has now been applied to the analysis of flow around moving fish.

It is well known to biologists that in the evolution of ray-finned fishes there are two clear evolutionary trends in pectoral fin design: the more derived the clade the more vertical is the inclination of the pectoral fin base (in basal clades it is nearly horizontal) and the more mid-dorsal is it's position on the fish's body (in basal clades the position of the fin is ventral) (Webb, 1982). Two fishes that represent these trends are the lower teleost rainbow trout (*Oncorhyncus mykiss*) and relatively lately derived perciform bluegill sunfish (*Lepomis macrochirus*). Using DPIV, direct measurements of the wake of these two freely swimming fish during unsteady maneuvring behaviors such as turning and breaking were obtained. This clarifies the functional significance of the transformation of pectoral fin morphology within the ray-finned fishes.

It was hypothesized that the basal orientation of the fin plays a role in the turning manoeuvre, and the position of the fin relative to the centre of mass of the fish is important

in the breaking manoeuvre. It was found that the laterally directed forces generated by vertically oriented pectoral fins during turning manoeuvers of the fish are significantly larger, because of their greater range of motion within the horizontal plane. On average the sunfish generated eight-times as much lateral force for turning as did the rainbow trout (Drucker and Lauder, 2002). This means that sunfish and other fish with vertical orientation of pectoral fins are able to turn faster than those with horizontal orientation and hence are better at manoeuvring.

During the breaking manoeuvre many ray-finned fishes extend their pectoral fins simultaneously to produce a retarding drag force (Drucker and Lauder, 2002). This manoeuvre creates a rolling or ''somersaulting'' momentum that compromises the stability of the fish, so it must counteract it with the motion of other posterior fins. It was found that for the sunfish, whose pectoral fin is more mid-dorsal and thus closer to the centre of the mass of the body this this ''somersaulting'' momentum was smaller and thus the breaking maneoeuvre more stable.

In conclusion it can be said that the experimental biomechanical approach has contributed significantly to our knowledge of fish locomotory mechanisms. Biomechanical insights can be used to construct evolutionary and ecological hypotheses about different fish species.

3.3. The contribution of this thesis and the advantages of computational fluid dynamics

In this thesis computational fluid dynamics (CFD) is used to simulate the flow around virtual models of sockeye salmon with varying dorsal hump sizes and calculate the drag force and coefficient acting on the models. For this the morphology of sockeye salmon is modified by increasing and decreasing the hump size. To the best of the author's knowledge the effect of differing morphologies in the same species of animals on the hydrodynamic drag has never been investigated before in CFD studies. This thesis thus is a novel application of the CFD method.

In the previous section the limitations of measuring rigid body drag were discussed. In this thesis comparative analysis between the morphologies of a fish in the same species and at the same life stage with differing hump morphologies is conducted. It can thus be assumed that these fish employ the same swimming modes. The morphologies with higher dead drag coefficients will thus face higher drag forces and be hydrodynamically disadvantaged. Although rigid body approximations cannot answer the question of the exact magnitude of the drag force that a swimming fish faces, the question of whether drag is increased, decreased or not impacted by varying hump size can be answered. In order to answer the question that this thesis poses the investigation of rigid models is thus sufficient.

Using CFD for the study of biological objects is advantageous for several reasons. The first is the controllability of experiments. For example morphological parameters of computer models of simulated animals can be easily modified. This is important because in a biological species there is a statistical distribution of morphometrics for every feature or trait in individuals of that species. Computer models of animals can be modified to represent different morphologies and size distributions of organisms. This leads to an increase in descriptive power of experimental data. To achieve the same results using real-life drag measurements one would have to obtain many individuals with differing morphologies, which can be difficult or impossible or alternatively construct models, which is more expensive and certainly less practical than simply modifying the models on a computer. In the case of this thesis using computer models was the only way to investigate

the hydrodynamics of sockeye salmon, because of the geographical remoteness of Estonia from the biological range of this species.

Another aspect of controllability emerges in simulations of moving fish. Here CFD is useful to study the hydrodynamics of different swimming modes and fish movements. In the case of real-life studies, such as DPIV, a major obstacle in experimentation is how to make a live fish follow the movement patterns required by the experiment. Experiment conditions can have an effects on fish such as stress that can impact their behavior and alter the results. In the case of CFD the fish can be programmed to follow any movement pattern specified by the programmer.

The second advantage of using CFD is from the view point of ethical questions regarding the experimentation on live animals, particularly where those experiments require the death of the animal in order to obtain valid scientific results. From the the ethical stand point infliction of pain or death upon an animal for scientific work should be avoided whenever possible. Some methods involved in the study of fish hydrodynamics can be cruel, for example Webb (1973) used partial caudal fin amputation to study to study whether that impaired the swimming of underyearling sockeye salmon. If the species that one wants to study is an endangered species, then using a method that is not fatal to the animal becomes extremely important, regardless of the ethical judgement of the experimenter. However information about their hydrodynamics can still be crucial, for example to find out whether the attachment of mechanisms to study these organisms such as radio-tracking transmitters will significantly add to their drag and thus impair them (as investigated in Obrecht et al, 1988).

Thirdly the experimental set up for real-life drag measurements inevitably leads to disruption in results due to the effect of the experiment equipment on the fluid flow, which means that often drag coefficients obtained by different research groups cannot be compared (Pennycuick, 1988; Sagnes et al, 2000). For example the tether or pole that the animal is attached to during the experiment can lead to flow effects that add to the drag of the model. The more streamlined the body is the more serious the problem of this ''interference drag'' (Vogel, 1994). Also the size of the wind or water tunnel can impact the outcome of the experiment, because it also has an effect on flow.

This section described the novelty of my methodology and the advantages of using CFD to answer the question of this thesis. In the following chapter, a detailed description of the method that will be used shall be provided.

4. MATERIALS AND METHODS

To investigate the subject of this thesis, the hydrodynamic impact of the male sockeye salmon's dorsal hump, five 3D computer models with varying hump sizes were simulated using computational fluid dynamics program OpenFoam.
In this chapter the detailed description of the method is given.

4.1. Preparation of the models

3D model of a sockeye salmon was obtained from Toucan Virtual Museum (ToucanMuseum). These models were modelled closely after photographs of sockeye salmon (e-mail correspondence with toco04@toucan.co.jp). The model was further modified using 3D modelling tool Blender 2.48. All of fins except the pectoral fin were removed. This is justified because as it was stated earlier, in this thesis the accurate drag coefficient of a moving sockeye salmon is not sought after. This thesis rather seeks to find the effect of the increase in hump size on drag. The models will comparable if the fins as the fins are removed from all of the models. The pectoral fins have a very different contribution to the drag of the entire body according to their orientation, so simulating them would only make sense if they were moving in a biologically accurate way.

The model was scaled to 60 cm in length from the tip of the nose to the tip of the tail of the fish (46.5 cm from mid-eye to the hypural bone). It was then modified by incrementally increasing/decreasing the hump size. As a result of this 5 models with differing aspect ratios (ratio between body length and body depth of the fish) were obtained.

Hump size was the only parameter that was modified, in all other aspects the models were identical. Through this comparability of the models with respect to hump size was achieved. The models were exported to stl format (stereolitography), which is the format accepted for meshing by OpenFOAM.

The quality of the stl model was checked using the surfaceCheck utility in OpenFOAM.

The reference area of the models for drag coefficient calculations was taken to be the surface area of the model. It was measured in Blender using the MeasureMesh script. In Table 4.1. with the body depths, aspect ratios and reference areas of models are given.

Body depth (cm)	**Aspect ratio**	**Reference area (cm^2)**
21.00	2.21	1750.50
19.50	2.38	1719.78
18.00	2.58	1670.12
16.50	2.82	1591.53
15.00	3.10	1520.35

Table 4.1. The measures of sockeye salmon models. Body depth here is the greatest distance from the hump to the belly normal to the lateral axis of the fish. Aspect ratio is the ratio of body length (measured from mid-eye to hypural bone of the fish models) to body depth.

In Figure 4.1. two models are illustrated. The rest of the models can be found in APPENDIX A.

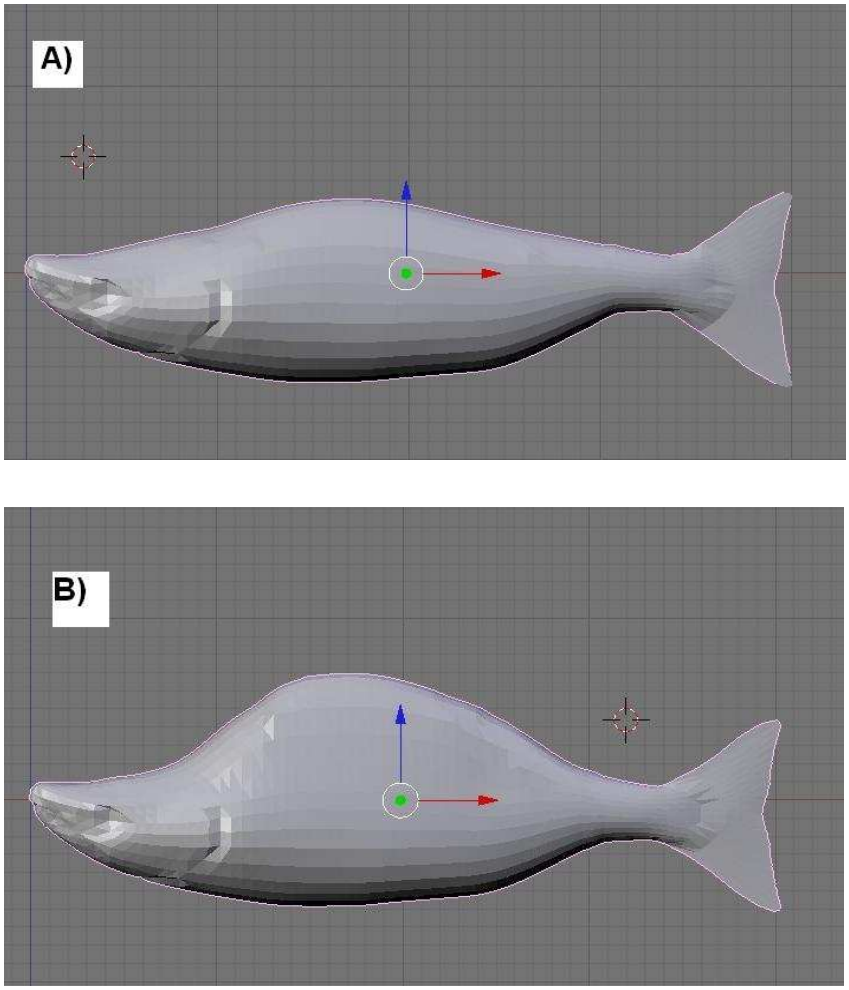

Figure 4.1. 3D models of sockeye salmon with aspect ratio A) 3.10 and B) 2.38.

4.2. Biological validation of the models

In order to ensure the biological validity of our results the dimensions of our models were compared to measurements of real sockeye salmon. Morphometric data for this comparison was obtained from Queen and Foote (1994). In the above article a beach spawning population that expressed extreme exaggeration of shape in males was studied. Morphological measurements of body length (distance from the middle of the eye to the hypural bone at the base of tail) and body depth (distance from the anterior insertion of the dorsal fin to the belly, perpendicular to the fish's long axis) were made on 164 males (here only 27 measurements are considered). In Figure 4.2. the morphometrics of biological fish are plotted along with the morphometrics of our models.

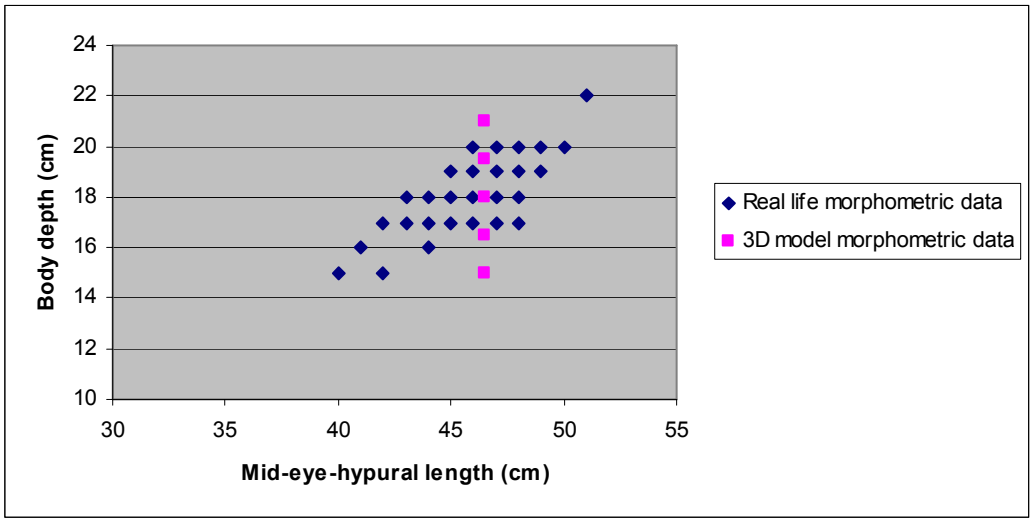

Figure 4.2. Comparison between morphometric data of real fish and the dimensions of the models

Figure 4.2. shows that most of our models are valid from the biological morphometric point of view, because they belong to the same measurement data cloud as do biological fish. To justify the models whose measurements don't directly belong to the cloud, two things can be said. First, because of the property of the law of similitude of *Re* number, our simulation results can be applied to individuals that are of a different size, but have the same geometry (this means that the free-stream velocity has to be adjusted to ensure the equality of *Re*). This means that the points corresponding to our models on Figure 4.2. can be shifted diagonally (changing the body depth and body length to the same extent). Secondly this data reprpesents only one biological population, in other populations the morphometrics of individuals could be considerably different. So the models that seem not to fit into this population could be common in another.

In the data of body depth information about the relative importance of hump length to belly depth has been lost and it isn't possible to control to what extent the measured fish corresponded to our models in that respect. However as the goal of this thesis is to investigate the impact of hump size on the drag coefficient rather than finding the accurate drag coefficients of biological sockeye salmon, this does not compromise my experiment or my ability to draw conclusions.

4.3. Computational fluid dynamics simulations

Models of sockeye salmon were simulated in OpenFOAM, an open-source computational fluid dynamics software. In this section an overview of the simulation process will be given.

The process of implementing CFD can be condensed into following steps:

1. Geometry input
2. Boundary conditions
3. Preprocessing
4. Calculation
5. Postprocessing

This section consists of the detailed description of each of these steps for my simulations.

4.3.1. Geometry input

In this stage the spatial domain of the simulation (or simply the space for which the calculations are performed) is defined and discretized into small cells. This discretized domain is called the mesh or the grid. This is neccessary because numerical solutions can give answers at only discrete points in the domain, called grid points. The domain for my simulation contained about 1.3 million cells.

The mesh needs to be more accurate near the boundaries where the no-slip condition applies, in our case the fish model is a no-slip wall. The further the boundary, the coarser the mesh gets. Before generating the mesh it is neccessary to calculate the minimum size of the cells near these boundaries in order to specify wall-functions. For this dimensionless wall distance (y^+) is considered. y^+ of the first cell outside the wall is required to be in the log layer, which depends on the Reynolds number of the simulation (OnlineCFD a). For the turbulence model used in our simulations, high-Re RANS model with wall functions, it is established that

30< y^+ < 200. y^+ is related to Δy (grid height near the no-slip wall) by the following equation:

$$y^+ = \Delta y \frac{u_\tau}{\nu}, \tag{4.1}$$

$$u_\tau = \sqrt{\frac{\tau_\varpi}{\rho}}, \tag{4.2}$$

and

$$\tau_\varpi = \rho \frac{C_f}{2} U^2 \tag{4.3}$$

where y^+ is dimensionless wall distance, u_τ (m/s) friction velocity, τ_ω (N/m^2) is the local wall shear stress and C_f (dimensionless) is skin friction coefficient. C_f can be found explicitly by equation (OnlineCFD d; Behrens 2009):

$$C_f = 0.0583\,\mathrm{Re}^{-0.2}$$

From these equations minimum grid size Δy for no slip condition boundaries can be calculated. My simulations were carried out with free stream velocities 0.5, 1, 2, 4. With y^+ chosen to be 100, the minimum grid size varies from 0.6 mm to 4 mm. A grid with Δy = *1mm* near the no-slip boundary was used in all the simulations.

Having calculated the Δy near no-slip boundaries the next step is to generate the mesh for the entire simulation. Mesh is created using OpenFOAM utilities. Initial, very coarse mesh is generated with blockMesh utility. The computational domain was defined to have dimensions of 1.5 m x 0.5 m x 0.5 m, which were divided correspondingly into 45, 15 and 15 pieces. After running the blockMesh a uniform mesh made out of cubicles with edge length $\Delta y \approx 33mm$ is obtained.

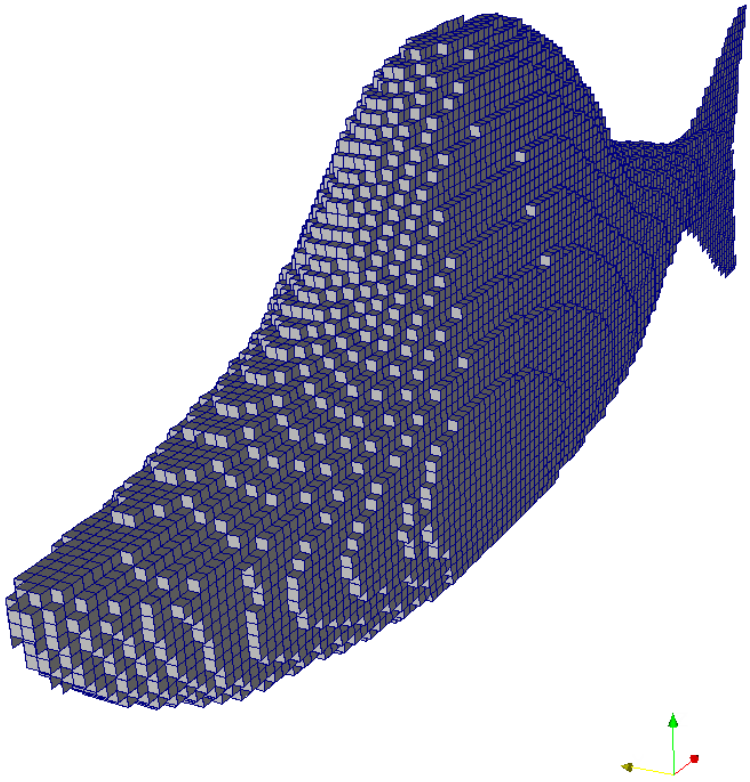

Figure 4.3. The mesh generated by blockMesh utility in OpenFOAM.

Fish model is inserted into this domain with snappyHexMesh utility as stl (stereo litography) surface. This utility creates an independent hexagon mesh, so the initial stl model is only used to define the surface of the computational mesh and isn't actually used in the simulation.

Then the surface of the mesh needs to be refined to satisfy the delta y calculated for no-slip boundaries in the beginning of this section. The first step for that is to refine cells, that are cut by the stl surface, to the level that is specified for the utility. If the goal is Δy = 1 mm on the boundary, the cells have to be refined 5 times. One refinement iteration bisects the cells in all dimensions. When the required refinement level for the object boundary is achieved the cells, that have more than 50% of their volume inside of the stl surface, are deleted. In next step snappyHexMesh utility tries iteratively snap the cells to the reference surface. At the end there may be cells that have multiple faces on the boundary, these faces can be concatenated.

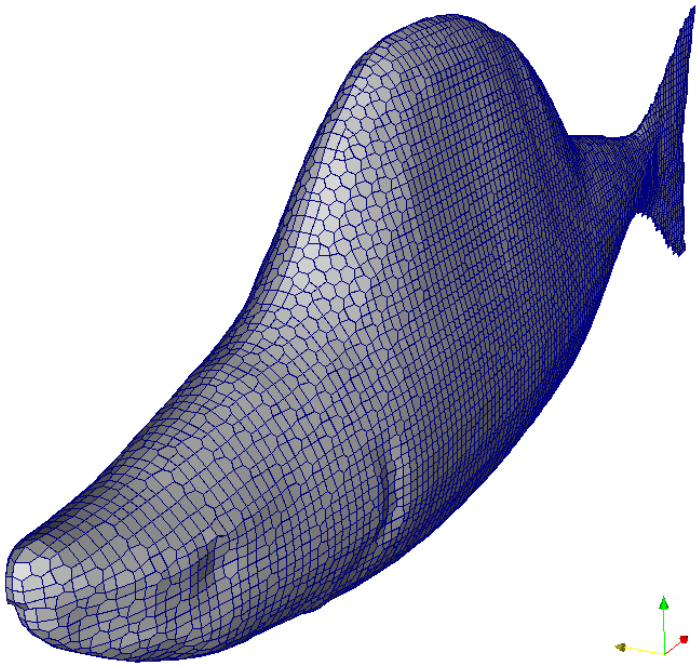

Figure 4.4. The mesh generated by snappyHexMesh utility in OpenFOAM.

Mesh quality is checked with checkMesh utility. Main parameters for mesh quality are aspect ratio and non-orthogonality. Aspect ratio is the ratio between cell edges. This should be close to 1. Non-orthogonality angle is the angle between face normals and a line that is between cell centers. The stability of the solution is affected by the face with the largest non-orthogonality angle. In the calculation phase the discretisation scheme for terms (especially the divergence and Laplacian terms) needs to be chosen taking into account the maximum non-orthogonality angle (OpenCFD, 2008).

4.3.2. Boundary conditions

At this stage it is specified how the flow near boundaries is to be treated. As mentioned in the previous section my simulation is set up in a domain with rectangular outer boundaries. There are thus 4 different types of boundaries in the simulation: inlet, outlet, edge of simulation domain and the no-slip wall (the fish mesh). The inlet is the outer boundary where the flow is considered to enter the simulation domain. Inlet is defined to have

uniform velocity with fixed value and zeroGradient pressure. The zeroGradient boundary condition sets the boundary value to the near-wall cell value. The outlet is the outer boundary where the flow leaves the simulation domain. Outlet lets fluid out with speed of free stream velocity and for any inflow component of velocity perpendicular to the boundary is cancelled out. At the edges of the simulation domain symmetryPlane boundary is used. This means that the area outside the simulation domain is considered to have identical flow to that of the cells adjacent to the boundary (these cells are effectively mirrored outside the boundary). This kind of boundary at the edges of the domain means that the domain is considered to be infinite. For the fish surface the no-slip Dirichlet boundary condition is used (OpenCFD, 2008).

4.3.3. Preprocessing

In the preprocessing stage the steady state solver potentialFoam is used to calculate the flow speeds in the simulation domain in order to use them as an initial value during the 0 time step. This avoids discontinuities in the simulation which would arise if the initial flow speed values of the simulation would be 0.

4.3.4. Calculation

In the calculation phase the governing equations of fluid dynamics (which were described in more depth in the Fluid Physics chapter) are discretized and solved within each of these cells or subdomains. In this section the governing equations of fluid dynamics and equations for turbulence modelling along with their numerical discretization scheme will be given.

4.3.4.1. Governing equations

CFD is based on the three fundamental principles governing the physics of any fluid flow: conservation of mass, Newton's second law and conservation of energy. These fundamental physical principles can be expressed in terms of mathematical equations.

These equations were expressed in the previous chapter in their most general forms in the section on fluid dynamics as either integral equations or partial differential equations. Here the governing equations of fluid dynamics are expressed in Cartesian tensor notation:

$$\frac{\partial u_i}{\partial x_i} = 0 \tag{4.4.}$$

$$\frac{\partial u_i}{\partial t} + u_j \frac{\partial u_i}{\partial x_j} = -\frac{1}{\rho}\frac{\partial p}{\partial x_i} + \upsilon \frac{\partial^2 u_i}{\partial x_j^2} \tag{4.5.}$$

$$\frac{\partial e_0}{\partial t} + u_j \frac{\partial e_0}{\partial x_j} = -\frac{1}{\rho}\left[u_j \frac{\partial p}{\partial x_j} + \frac{\partial q_j}{\partial x_j} \right] + \upsilon u_i \frac{\partial^2 u_i}{\partial x_j^2} \tag{4.6.}$$

where e_0 (J) is total energy and q (W/m^2) is heat flux.

Since I am not interested in heat transfer I assume that the temperature is constant and energy equation is not important in my simulations.

Reynolds averaged Navier-Stokes (RANS) equations are used for turbulence modelling. These are time-averaged equations for motion of fluid flow that are derived from regular Navier-Stokes equations. To derive these equations the flow variables are decomposed into two parts: the mean (time-averaged) component and the fluctuating component. Here they are given in tensor notation:

$$\frac{\partial U_i}{\partial x_i} = 0 \tag{4.7}$$

and

$$\rho\left[\frac{\partial U_i}{\partial t} + U_j \frac{\partial U_i}{\partial x_j} \right] = -\frac{\partial P}{\partial x_i} + \frac{\partial}{\partial x_j}\left[T_{ij} - \rho\left\langle u_i u_j \right\rangle \right]. \tag{4.8}$$

In these equations capital letters for velocity, pressure and stress tensor represent mean or average motion and lower case letters fluctuating motion (OnlineCFD c).

RANS is a popular turbulence modelling approach, because it is relatively inexpensive even for complex flow configurations and can account for viscous effects. The main limitation of the approach is that it provides information only about the largest flow structures (Mittal, 2004). This becomes a problem when smaller flow structures affect the behavior of larger vortex structures in real flow and hence their lack in the simulation makes the result less realistic. Because my simulations were conducted at high Re, it was judged that RANS turbulence modelling gives a sufficiently accurate picture of flow.

In the solution of high-Re RANS wall functions are used, here *k*- ε turbulence model is implemented. In this model new variables are introduced to the RANS equations. *k* is the average fluctuating kinetic energy per unit mass and ε is the rate of dissipation of turbulence kinetic energy per unit mass due to viscous stresses. The here *k*- ε model is described by following equations:

$$\mu_T = \rho C_\mu \frac{k^2}{\varepsilon}, \tag{4.9}$$

$$\rho\left[\frac{\partial}{\partial t} + U_j \frac{\partial}{\partial x_j}\right]k = \frac{\partial}{\partial x_j}\left[\left(\mu + \frac{\mu_T}{\sigma_k}\right)\frac{\partial k}{\partial x_j}\right]T_{ij}\frac{\partial U_i}{\partial x_j} - \rho\varepsilon, \tag{4.10}$$

$$\rho\left[\frac{\partial}{\partial t} + U_j \frac{\partial}{\partial x_j}\right]\varepsilon = C_{\varepsilon 1}\frac{\varepsilon}{k}T_{ij}\frac{\partial U_i}{\partial x_j} - C_{\varepsilon 2}\rho\frac{\varepsilon^2}{k} + \frac{\partial}{\partial x_j}\left[\left(\mu + \frac{\mu_T}{\sigma_\varepsilon}\right)\frac{\partial \varepsilon}{\partial x_j}\right], \tag{4.11}$$

$$k = \frac{1}{2}\langle u_i u_i \rangle = \frac{1}{2}\langle q^2 \rangle = \frac{1}{2}\left[\langle u_1^2 \rangle + \langle u_2^2 \rangle + \langle u_3^2 \rangle\right] \tag{4.12}$$

and

$$\varepsilon = 2\upsilon\langle s_{ij} s_{ij} \rangle, \tag{4.13}$$

where μ_T represents eddy viscosity, s_{ij} represents strain-rate tensor and C_μ, $C_{\varepsilon 1}$, $C_{\varepsilon 2}$, σ_k, σ_ε are closure coefficients (OnlineCFD e; Wilcox, 2006).

4.3.4.2. Numerical method

In order to solve the governing equations computationally in CFD, integrals or the partial derivatives in these equations are replaced with discretized algebraic forms, which are solved by the computer to obtain the numerical flow field values at discrete points in time and/or space (Andersson, 1995). This process is called discretization. It means that we can obtain values of the physical parameters of the flow such as velocity, pressure and vorticity for discrete points in the simulation at discrete timesteps.

In this thesis simulations are carried out using Finite Volume Method (FVM). In FVM volume integrals over small volumes surrounding each node point in a mesh, that contain a divergence term are converted to surface integrals, using the divergence theorem (Andersson, 1995). These surface integral terms are then calculated as fluxes at the surface of each finite volume. FVM does not depend on structure of the mesh because it calculates field values in cell centers. This means that the fact that after mesh refinement with snappyHexMesh utility the mesh is not uniform and cells near the boundary of the fish have arbitrary shapes, does not impact the quality of simulations.

In OpenFOAM discretization and interpolation schemes can be specified for every term: time, divergence, Laplacian terms etc. This is done in configuration file fvSchemes. As was mentioned above the choice of discretization schemes has to be done with taking the quality of the mesh into account. This is because discretization scheme depends on the stability of the solution which in turn is affected by quality of the mesh.

In addition to discretization schemes user can also choose linear solvers, tolerances and preconditioners for every variable in the system of equations solved. Preconditioners are used to get system convergence faster. They lead to a faster propagation of information through the computational mesh. Linear solvers act iteratively, they base on reducing the

equation residual over a succession of solutions. The solver stops when the residual falls below solver tolerance or the ratio of current to initial residuals falls below the solver relative tolerance relTol. A complete list of linear solvers and preconditioners can be found in OpenCFD (2008) and Behrens (2009).

Most unsteady flow solver applications in OpenFOAM also use the pressure-implicit split-operator (PISO) scheme. PISO is used for transient solvers and the purpose of this scheme is to make corrections in equation variables. It also makes corrections to account for mesh non-orthogonality (Wütrich, 2007).

4.3.5. Postprocessing

4.3.5.1. Calculation of drag force and coefficient

Drag force along x_1 direction can be computed by integrating pressure and viscous forces acting on the body as follows:

$$D = \int_A (-pn_1 + \tau_{1j} n_j) dA . \tag{4.14}$$

Here n_i is the i-th component of the unit normal vector on surface dA and τ_{ij} is the viscous stress tensor.

OpenFOAM can calculate drag force automatically or in postprocessing by utility execFlowFunctionObjects. This utility also calculates drag coefficient using predefined free stream velocity U and reference area A (the reference areas for our models were given in the section ''Preparation of models''):

$$C_d = \frac{D}{\frac{1}{2}\rho A U^2} . \tag{4.16}$$

4.3.5.2. Data processing

The values of drag forces and drag coefficients were obtained for every time step in the simulation. The averages and standard deviations were calculated in Excel using Excel functions. The results for initial timesteps of the simulation were not included in the calculation of average force and standard deviation as during the initial timesteps, the forces have not yet converged and deviate significantly from the value that can be considered reliable.

4.3.5.3. Simulation visualization

Simulation visualization for the speed 2 m/s for the sockeye models with aspect ratio 2.38 and 2.82 were created using the program paraView and the script paraFOAM. Simulation visualization is presented in the chapter "Results".

4.4. Validation of the CFD method

In order to validate our results we compare the drag coefficient we obtain through CFD with experimental data of drag coefficient of the sphere.

Sphere diameter was set to be 0.08 m and free-stream flow velocity of the simulation was 1 m/s, which means that the simulation was performed at Re = 80000. This Re is particularly well suited to use for validation because the curve of the drag coefficienct of the $Re = 10^4 – 10^5$. The experimental data of drag coefficient corresponding to these Re is $C_d = 0.39 – 0.52$ (Blevins, 2003).

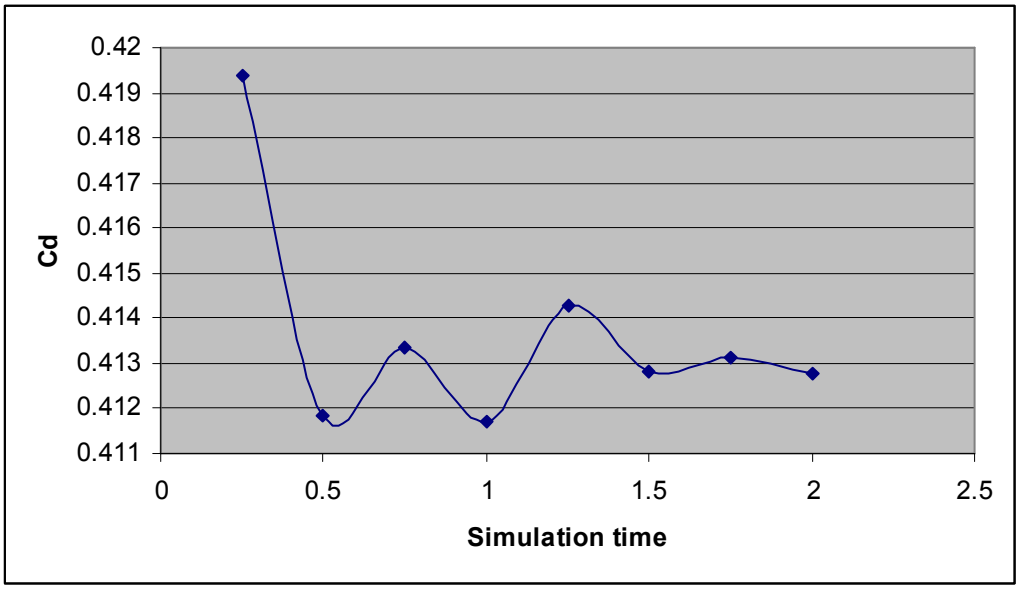

Figure 4.5. Drag coefficient of the sphere versus simulation time.

Figure 4.5. shows how the values of drag coefficent value converges to value 0.413 in the course of the simulation. The initial timesteps are always subject to fluctuation and instabilities, but as the simulation progresses the value stabilizes. Because of the arbitrary skin friction of the models C_d is assumed to drop to the lower end of the experimental data range, but this drop of C_d is not influential to the simulations data of the fish because all models are with same skin friction. The drag coefficient that was obtained fits into experimental data, this provides proof that our simulations are physically correct.

5. RESULTS

5.1. Drag forces and drag coefficients

The drag coefficients and drag forces obtained from the simulations showed the relationship that the bigger the hump of the sockeye (the smaller the aspect ratio) the bigger the drag forces and coefficients.

Below the results are presented. Graphs for drag force and drag coefficient plotted against free-stream velocity is provided in APPENDIX B.

	Reynolds numbers			
Aspect ratio	**300000**	**600000**	**1200000**	**2400000**
2.21	0.4420±0.0002	1.2136±0.0006	3.7464±0.0049	12.4782±0.0197
2.38	0.4159±0.0001	1.1364±0.0006	3.5028±0.0024	11.6793±0.0190
2.58	0.3836±0.0001	1.042±0.0006	3.2079±0.0022	10.6648±0.0178
2.82	0.3454±0.0001	0.9321±0.0005	2.8732±0.0040	9.5666±0.0244
3.10	0.3244±0.0001	0.8765±0.0005	2.7048±0.0038	9.0023±0.0230

Table 5.1. Drag forces and their standard deviations

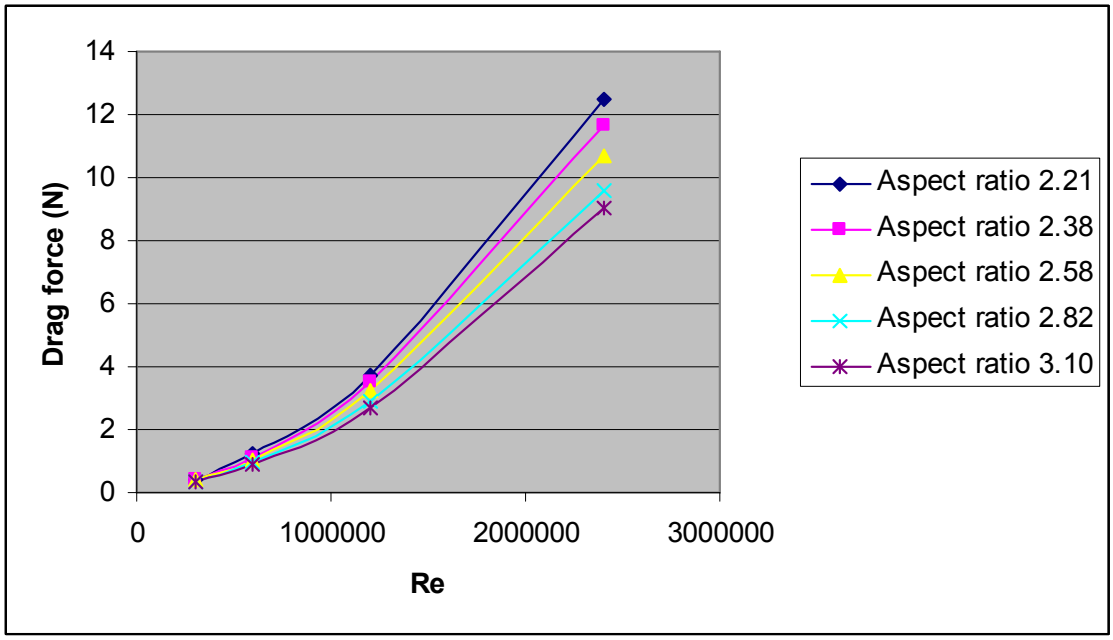

Figure 5.1. Drag forces plotted against the Re of the simulation

	Reynolds number			
Aspect ratio	300000	600000	1200000	2400000
2.21	0.0202±0.0001	0.0138±0.0001	0.0107±0.0002	0.0089±0.0002
2.38	0.0193±0.0001	0.0132±0.0001	0.0101±0.0001	0.0084±0.0002
2.58	0.0183±0.0001	0.0124±0.0001	0.0096±0.0001	0.0079±0.0002
2.82	0.0173±0.0001	0.0117±0.0001	0.0090±0.0002	0.0075±0.0003
3.10	0.01707±0.0001	0.0115±0.0001	0.0088±0.0002	0.0074±0.0003

Table 5.2. Drag coefficients and their standard deviations

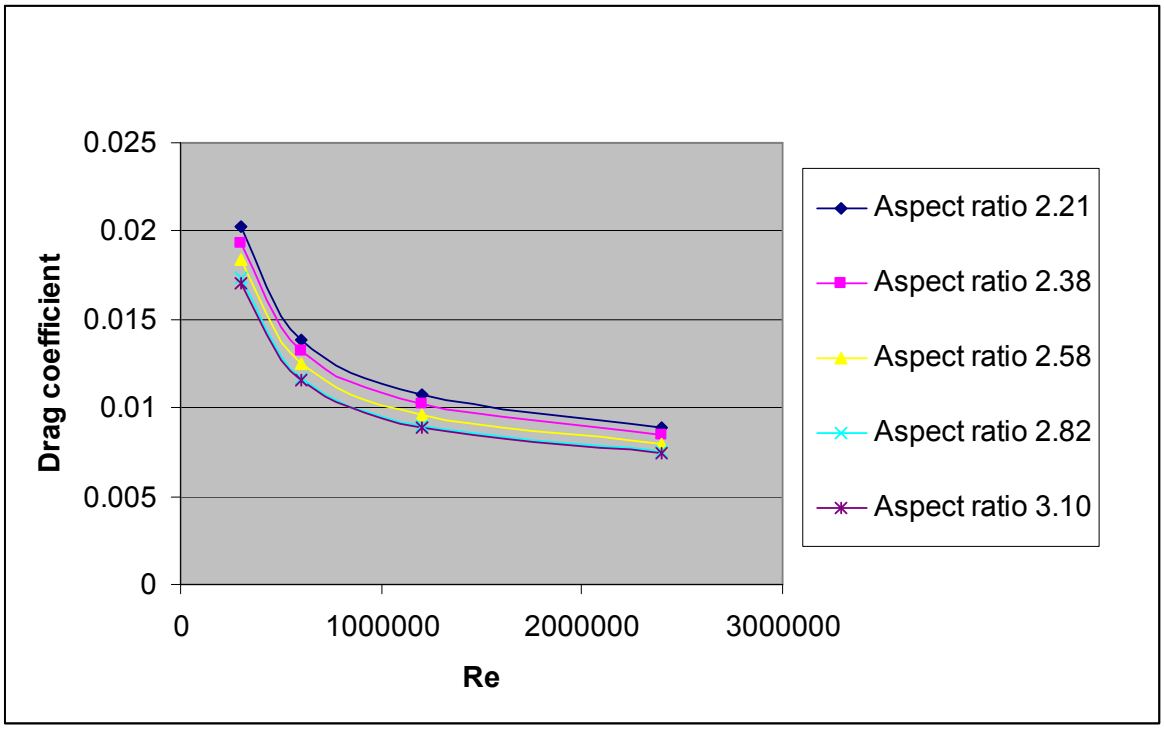

Figure 5.2. Drag coefficients plotted against the Re of the simulation

Figure 5.3. was made for comparative purpsoses. I took the drag forces acting on the model with aspect ratio 2.58 for every *Re* to be the reference values and calculated by how many percents the drag force values differed for the other models at each simulated *Re*.

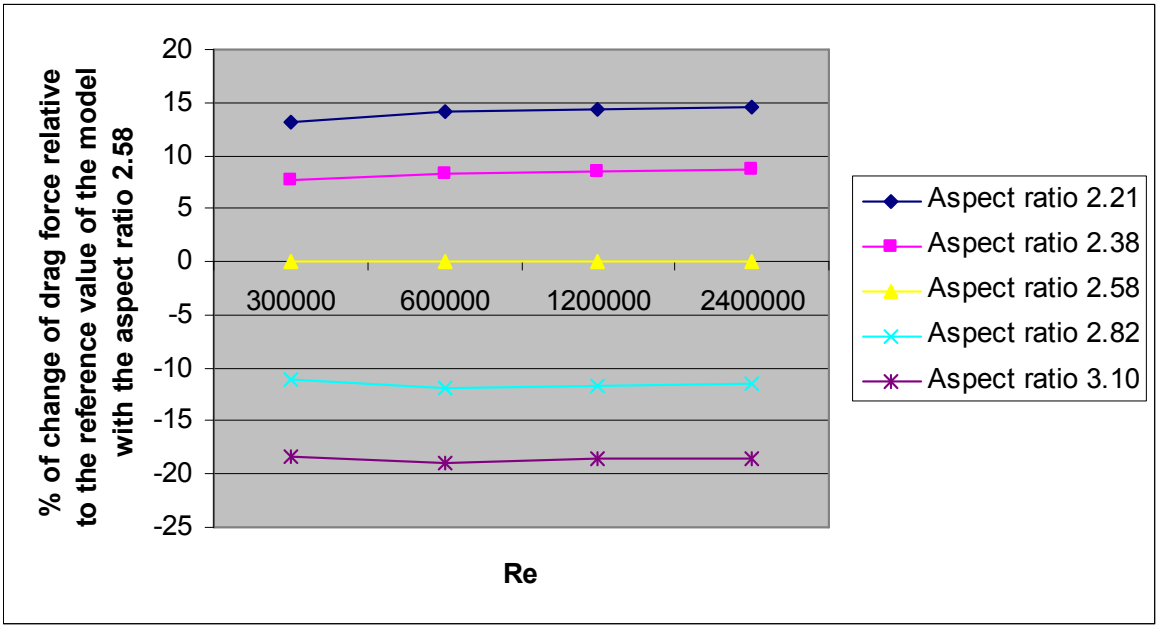

Figure 5.3. % of difference of drag force relative to the model with the aspect ratio 2.58 for each of the models plotted for every simulated Re

5.2. Energetics calculations

In Figure 5.4. thrust power required to overcome the drag force is calculated using the equation 3.3. To swim the fish needs to produce thrust force that is higher or equal to the drag force acting on the fish. By velocity we mean the velocity of the fish relative to the fuid. The reference frame can be connected wit either the water or the fish, this doesn't impact the physics of flow.

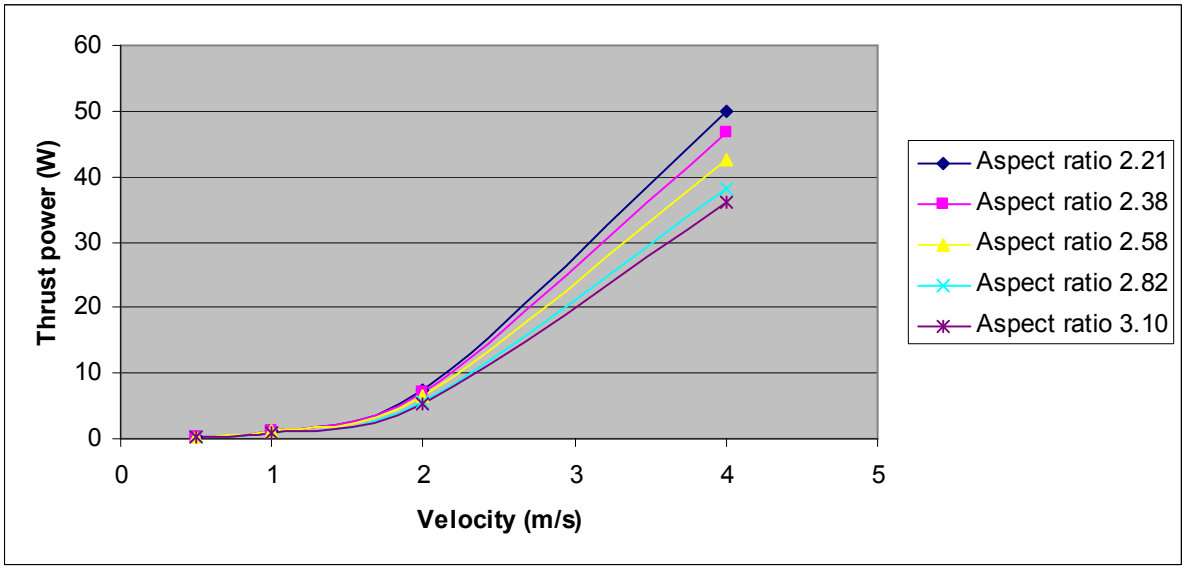

Figure 5.4. Thrust power plotted against simulation velocities.

In figure 5.5. and 5.6. work is calculated according to the equation 3.2.

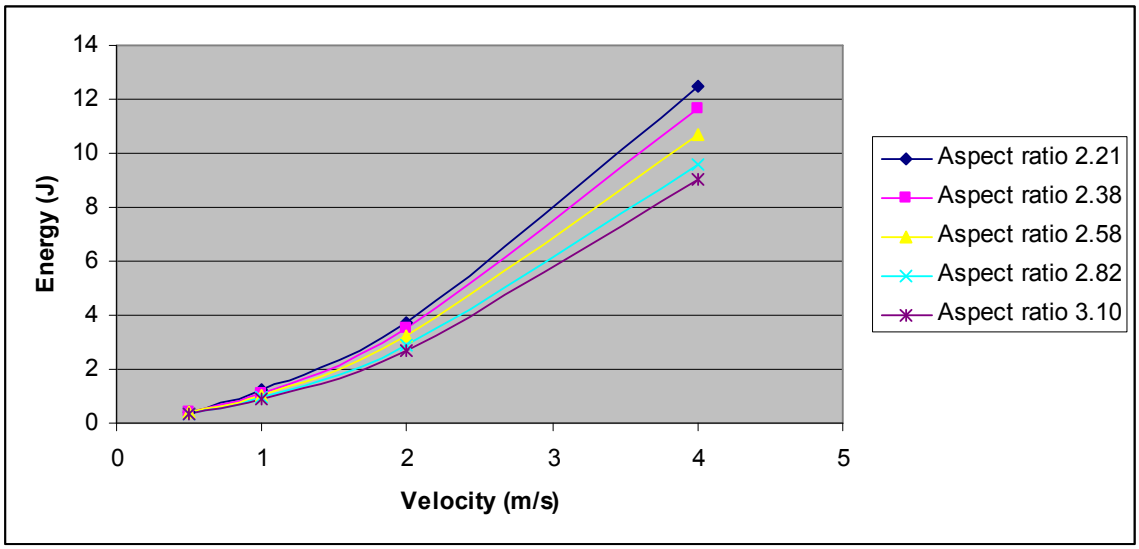

Figure 5.5. Work required to swim 1 m plotted against simulation velocities.

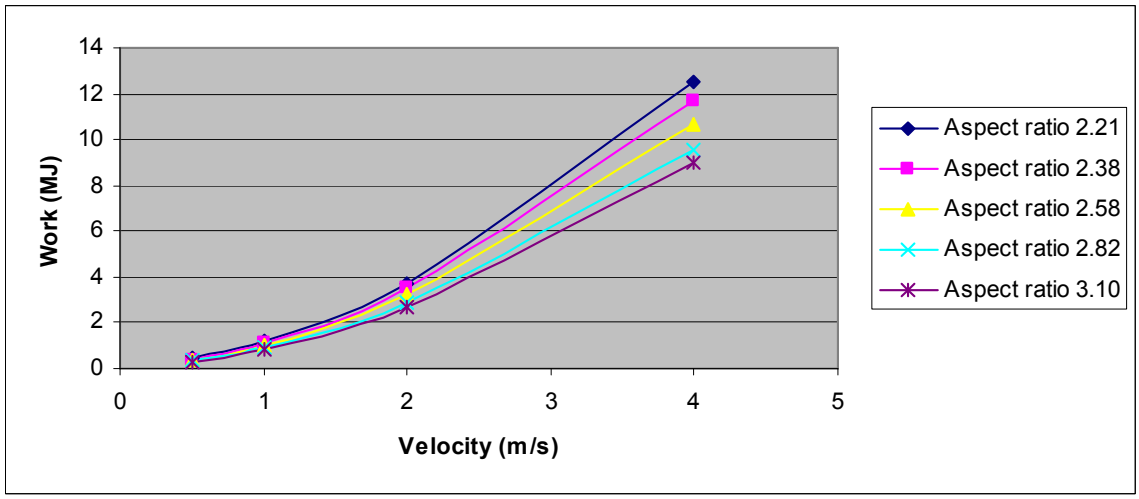

Figure 5.6. Work required to swim 1000 km plotted against simulation velocities.

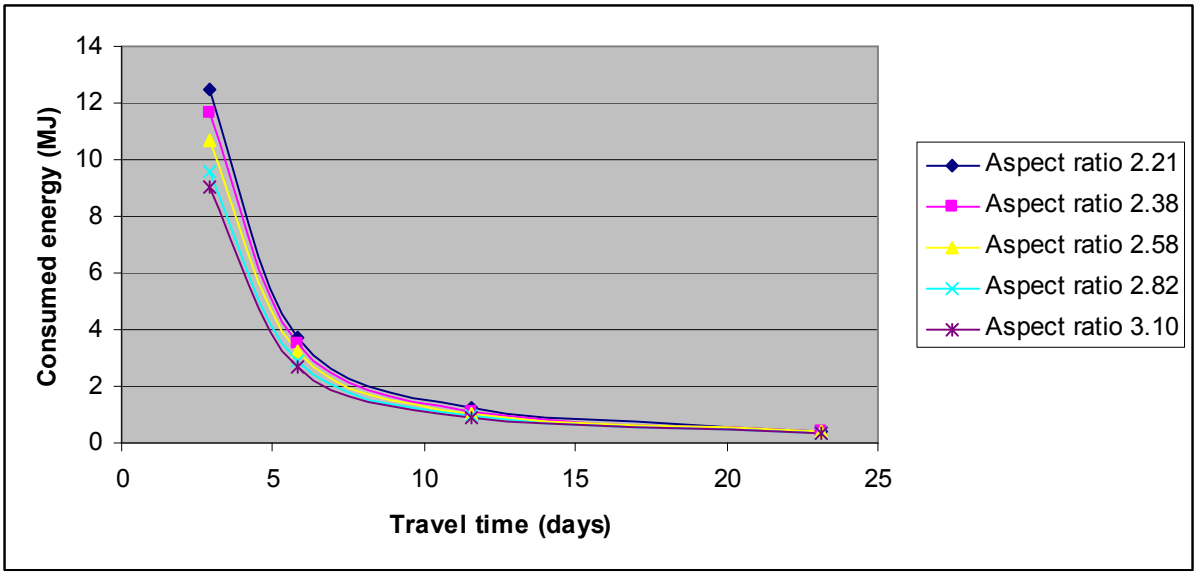

Figure 5.7. Energy requirement (work) plotted versus travel time of 1000 km

5.3. Flow visualization

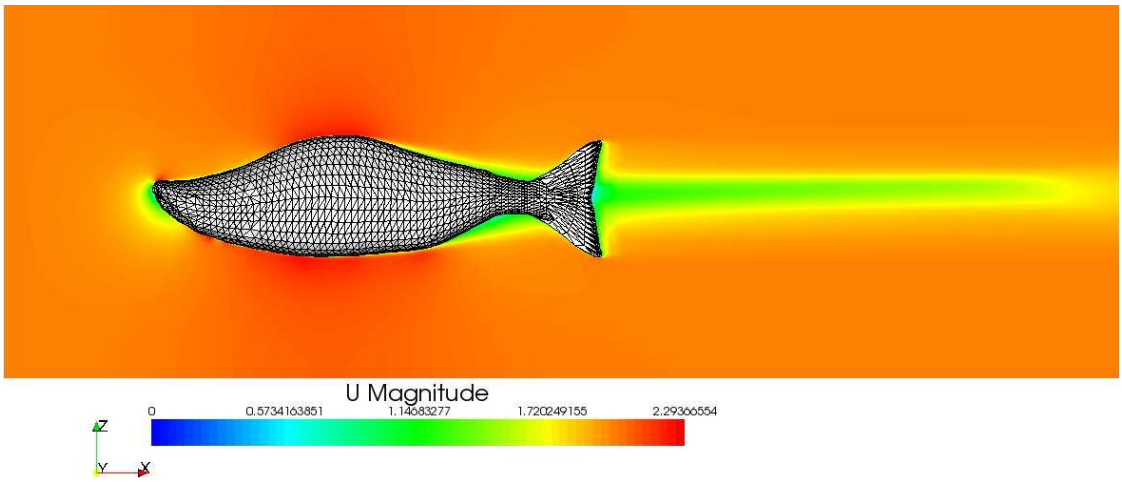

Figure 5.8. Velocity field around the sockeye salmon with aspect ratio 2.82 at free-stream velocity of 2 m/s. Units are in m/s.

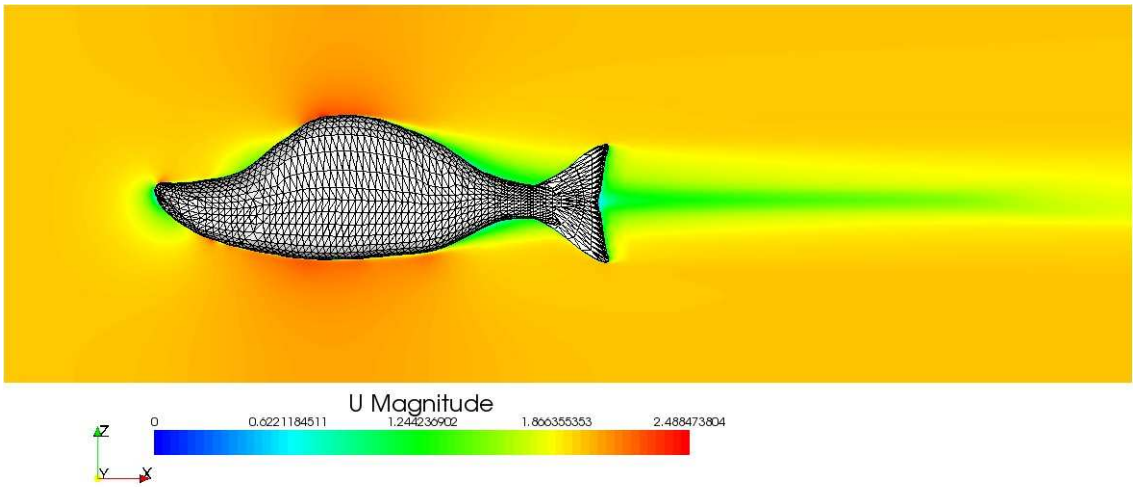

Figure 5.9. Velocity field around the sockeye salmon with aspect ratio 2.38 at free-stream velocity of 2 m/s. Units are in m/s.

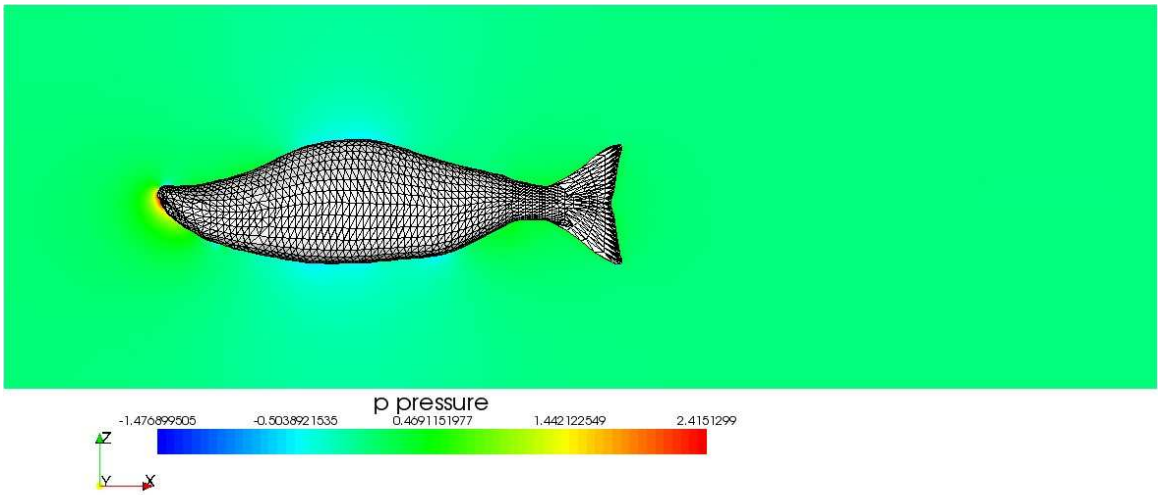

Figure 5.10. Pressure field around the sockeye salmon with aspect ratio 2.82 at free-stream velocity of 2 m/s. Units are in Pa.

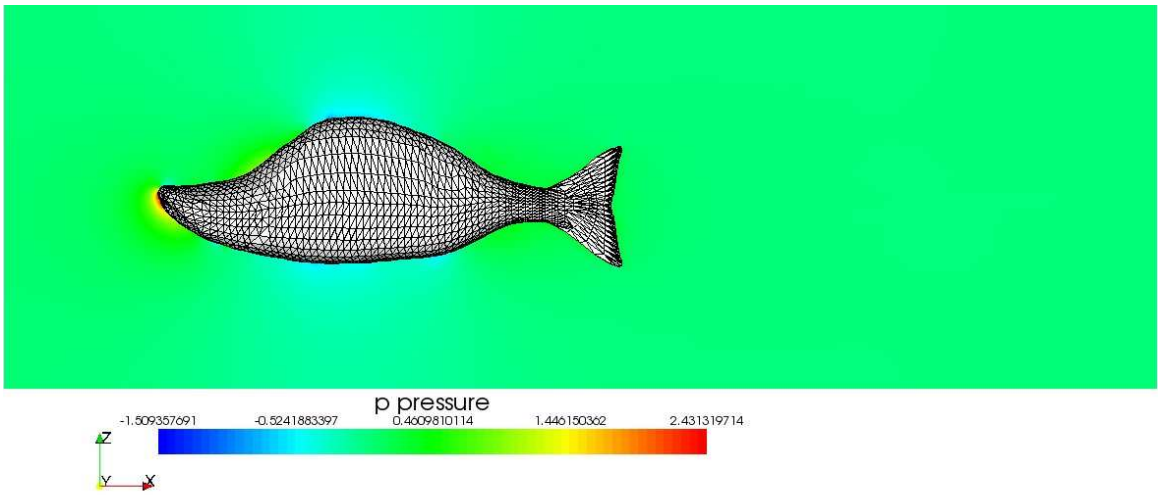

Figure 5.11. Pressure field around the sockeye salmon with aspect ratio 2.38 at free-stream velocity of 2 m/s. Units are in Pa.

6. DISCUSSION

6.1. Relationship between drag force and drag coefficient and hump size

Simulation results presented in the previous chapter show that a bigger hump corresponds to a larger hydrodynamic drag force acting on the body and a larger non-dimensional drag coefficient for each of the simulated *Re*. The drag force and drag coefficient behaved consistently, there were no irregular results. These results prove the hypothesis of this thesis that individuals with larger humps face higher drag force. Figure 5.3. shows that the model with the biggest hump (lowest aspect ratio) was subject to nearly 35% more drag force than the relatively streamlined model with the smallest hump (highest aspect ratio). Because work is drag force multiplied by distance, Figure 5.3. also describes the energetic requirements of swimming. This means that the model with the biggest hump would have to expend 35% more energy

6.2. Relationship between hump size and the energetic requirements of swimming

Figure 5.7. elucidates that males with bigger humps have to expend more energy to reach the spawning grounds at the same time as males with smaller humps.
The energy that has to be expended to decrease travel time increases nonlinearly. This sets a realistic limit on how fast a fish can cross a certain distance.

6.3. What can be inferred from flow visualization results?

Because our simulations were done using RANS turbulence modelling, which averages pressure and other parameters of flow, some finer features like vortex structures are not visualized. However it is still possible to make conclusions about the general properties of flow.

Figure 5.9. has a bigger wake compared to Figure 5.8. From this it can already be inferred that the model with the larger hump distorts the flow more and should thus have a bigger drag.

6.4. Reliability

The standard deviations for our simulation results were small, which means that the obtained solutions were stable. Also our method was validated by comparing CFD results for a sphere with experimental data, where the drag coefficient of drag was measured using real-life methods.

CONCLUSION

This thesis aimed at proving the hypothesesis that the hump increases the drag of the sockeye salmon. As the body of the male becomes less streamlined with the increase of the hump, there was reason to believe that this indeed would be the case. However this hypothesis has never been investigated experimentally. To test this hypothesis, computational fluid dynamics was used to simulate the flow around sockeye salmon models with different hump sizes at four different *Re* (free-stream velocity was modified). The results showed that a bigger hump corresponds to bigger drag and drag coefficient for every *Re*. The hypothesis of this thesis was thus proven to be true.

Because of the increased drag a male with a bigger hump has to produce more thrust and thus expend more energy to achieve the same swimming speed compared to a male with a smaller hump. Because the male dorsal hump subject to sexual selection, these results mean that there exists a tradeoff between hydrodynamic efficiency and reproductive success in sockeye salmon species. Larger energy requirements is the price that a male must pay for the advantage over other males in courtship. Energy however is a limited resource for sockeye, because they stop eating once they enter freshwater and start their migration upstream. Once consumption of energy reaches about 4 MJ/kg the sockeye will die. So for

some individuals this price may be too high and they will perish along the journey from energy exhaustion.

Because of the limited energetic budget the hydrodynamic drag affects the probability of a sockeye salmon to reach the spawning site (among other factors such as bear predation etc.). This probability is thus a decreasing function of hump size, meaning that the larger the hump the smaller the probability to reach the spawning site. However the impact of the drag on this probability will depend on the length of the journey and river hydraulics. Our results showed that the faster the free-stream velocity the greater is the difference in drag forces acting on a sockeye with different hump sizes and thus the more disadvantaged the individuals with greater humps are.

However once the sockeye reaches the spawning grounds his probability of leaving behind progeny will be an increasing function of the hump size, so the individuals with larger humps are likely to leave behind more offspring. It is interesting that a single trait can have both a positive and a negative impact on the fitness of the organism (its likelihood to leave behind offsprings).

By looking at the new generation it can be assessed which factor contributed more to mating success— the energetic efficiency or attractiveness to females. The relative importance of natural and sexual selection on the hump size for different populations can be assessed. This explains why individuals in different populations can have drastically varying hump sizes. Because the selective pressure for the trait is dependent not only on sexual selection, where females always prefer the male with a larger hump, but also on population specific factors like fluid velocity and migration distance, this trait will vary in different populations.

The biomechanical approach used in this thesis was effective in elucidating the role of the dorsal hump in biological fitness of the sockeye salmon. Biomechanics is of growing importance in many fields of biology, because it provides useful tools for the analysis of physical functions in organisms and that can lead to novel insights into how animals perform functions and adapt to their environment and how species evolve.

REFERENCES

Anderson, J. D. Jr. 1995. Computational Fluid Dynamics: The Basics with Applications. McGraw-Hill, Inc.

Andersson, M. B. 1994. Sexual selection. Princeton University Press, Princeton.

Aono, H., Liang, F., Liu, H. 2008. Near- and far-field aerodynamics in insect hovering flight: an integrated computational study. *J. Exp. Biol*., **211**, 239-257.

Barrett, D. S., Triantafyllou, M. S., Yue, D. K. P., Grosenbaugh, M. A., Wolfgang, M. J. 1999. Drag reduction in fish-like locomotion. *J. Fluid Mech*., **392**, 183-212.

Behrens, T. 2009. OpenFOAM's basic solvers for linear systems of equations. Solvers, preconditioners, smoothers. 2009. [Online] http://www.tfd.chalmers.se/~hani/kurser/OS_CFD_2008/TimBehrens/tibeh-report-fin.pdf (27.05.09)

Berejikian, B. A., Tezak, E. P., LaRae, A. L. 2000. Female mate choice and spawning behaviour of chinook salmon under experimental conditions. *Journal of Fish Biology*, **57**, 647-661.

Biewener, A. 2003. Animal locomotion. Oxford University Press, USA.

Blevins, R. D. 2003. Applied Fluid Dynamics Handbook. Krieger Publishing Company Malabar, Florida.

Bilo, D., Nachtigall, W. 1980. A simple method to determine drag coefficients in aquatic animals. *J. Exp. Biol*., **87**, 357-359.

Borazjani, I., Sotiropoulos, F. 2008. Numerical investigations of the hydrodynamics of carangiform swimming in the transitional and inertial flow regimes. *J. Exp. Biol*., **211**, 1541-1558

Borazjani, I., Sotiropoulos, F. 2009. Numerical investigations of the hydrodynamics of anguilliform swimming in the transitional and inertial flow regimes. *J. Exp. Biol*., **212**, 576-592.

Brett, R. J. 1995. Energetics. In ''Physiological Ecology of Pacific Salmon'' (Groot, C., Margolis, L., and Clarke, W. C., Eds.), pp. 1-68. UBC Press, Vancouver

Bushnell, D. M. 1991. Drag reduction in nature. *Annu. Rev. Fluid Mech*., **23**, 65-79.

Chaplin, M. Water structure and science: Hydrocolloid rheology. [Online] http://www.lsbu.ac.uk/water/hyrhe.html (24.05.09)

Cooke, S. J., Hinch, S. G., Crossin, G. T., Patterson, D. A., English, K. K., Healey, M. C., Shrimpton, J. M., Van der Kraak, G., Farrell, A. P. 2006. Mechanistic basis of individual mortality in Pacific salmon during spawning migrations. Ecology, **87 (6)**, 1575-1586

Crossin, G. T., Hinch, S. G., Farrell, A. P., Higgs, D. A., Lotto, A. G., Oakes, J. D., Healey, M. C. 2004. Energetics and morphology of sockeye salmon: effects of upriver migratory distance and elevation. Journal of Fish Biology, **65**, 788-810

Crossin, G. T., Hinch, S. G., Farrell, A. P., Whelly, M. P., Healey, M. C. 2003. Pink salmon (Onchorhynchus gorbuscha) migratory energetics: Response to migratory difficulty and comparisons with sockeye salmon (Onchorhynchus nerka). *Can. J. Zool*. **81**, 1986-1995

Darwin, C. 1871. The Descent of Man and Selection in Relation to Sex. [Online] http://www.gutenberg.org/dirs/etext00/dscmn10.txt (17.05.2009)

Darwin, C. 1859. The Origin of Species. Oxford University Press, Oxford (Published in 1998), p. 73.

Dickerson, B. R., Brinck, K. W., Willson, M. F., Bentzen, P., Quinn, T. P. 2005. Relative importance of salmon body size and arrival time at breeding grounds to reproductive success. *Ecology*, **86 (2)**, 347-352

Dobzhansky, T. 1973. Nothing in biology makes sense except in the light of evolution. *The American Biology Teacher.*

Drucker, E. G., Lauder, G. V. 2002. Wake dynamics and locomotor function in fishes: interpreting evolutionary patterns in pectoral fin design. *Integr. And Comp. Biol*, **42**, 997-1008.

Fishbase. Fishbase: Sockeye salmon. [Online] http://www.fishbase.org/Summary/SpeciesSummary.php?id=243 (24.05.09)

Foote, C. J., Larkin, P. A. 1988. The role of male choice in the assortative mating of anadromous and non-anadromous sockeye salmon (*Oncorhynchus nerka*). *Behaviour*, **106**, 43-62

Ghiselin M. T. 1974. The Economy of Nature and the Evolution of Sex. University of California Press, Berkeley & London.

Gustafson, R. G., Wainwright, T. C., Winans, G. A., Waknitz, F. W., Parker, L. T., Waples, F. W. Status review of sockeye salmon from Washington and Oregon. Life history of *Oncorhynchus nerka*. NOAA Technical Memorandum NMFS-NWFSC-33,

National Marine Fisheries Service. 1997. [Online] (http://www.nwfsc.noaa.gov/publications/techmemos/tm33/life.html) (17.05.2009)

Hamon, T. R., Foote, C. J. 2005. Concurrent natural and sexual selection in wild male sockeye salmon, Oncorhynchus nerka. *Evolution*, **59(5),** 1104-1118

Healey, M. C., Lake, R., Hinch, S.G. 2003. Energy expenditures during reproduction by sockeye salmon (Onchorhynchys nerka). *Behaviour*, **140**, 161-182

Hendry, A. P., Berg, O. K. 1999. Secondary sexual characters, energy use, senescence and the cost of reproduction in sockeye salmon. *Can. J. of Zool.,***77,** 1663-1775

Hendry, A. P., Quinn, T. P. 1997. Variation in adult life history and morphology among Lake Washington sockeye salmon (Onchorhynchys nerka) populations in relation to habitat features and ancestral affinities. *Can. J. Fish. Aquat. Sci*., **54**, 75-84

Hinch, S. G., Cooke, S. J., Healey, M. C., Farrell, A. P. (Tony). 2006. Behavioural physiology of fish migrations: Salmon as a model approach. Behaviour and Physiology of fish, volume 24. Elsevier.

Hinch, S. G., Standen, E. M., Healey, M. C., Farell, A. P. 2002. Swimming patterns and behaviour of upriver-migrating adult pink (*Oncorhynchus gorbuscha*) and sockeye (*O. nerka*) salmon as assessed by EMG telemetry in the Fraser River, British Columbia, Canada. *Hydrobiologia*, **483**, 147-160.

Homsy, G. M., Aref, H., Breuer, K. S., Hochbreb, S., Koseff, J. R., Munson, B. R., Powell, K. G., Robertson, C. R., Thoroddsen, T. S. 2000. Multimedia Fluid Mechanics. Cambridge University Press.

Koehl, M. A. R. 1996. When does morphology matter? *Annu. Rev. Ecol. Syst*., **27**, 501-542.

IUPAC a. IUPAC Gold Book: Viscosity. [Online]
http://goldbook.iupac.org/V06627.html (19.05.2009)

IUPAC b. IUPAC Gold Book: Dynamic viscosity. [Online]
http://goldbook.iupac.org/D01877.html (19.05.2009)

IUPAC c. IUPAC Gold Book: Shear stress. [Online]
http://goldbook.iupac.org/S05638.html (19.05.2009)

IUPAC d. IUPAC Gold Book: Kinematic viscosity. [Online]
http://goldbook.iupac.org/K03395.html (19.05.2009)

Lane, D.M., Stafiotakis, M., Davies, J. B. C. 1998. Review of fish swimming modes for aquatic locomotion. IEEE Journal of Oceanic Engineering, 24-2, 237-352

Lin, J., Quinn, T. P., Hilborn, R., Hauser, L. 2008. Fine-scale differentiation between sockeye salmon and the effect of phenotype on straying. *Nature Heredity*, **101**, 341-350

Liu, H., Wassersug, R. J., Kawachi, K. 1996. A computational fluid dynamics study of tadpole swimming. *J. Exp. Biol*., **199**, 1245-1260.

Liu, H., Wassersug, R., Kawachi, K. 1997. The three-dimensional hydrodynamics of tadpole locomotion. *J. Exp. Biol*., **200**, 2807-2819.

Lovvorn, J. R., Jones, D. R., Blake, R. W. 1991. Mechanics of underwater locomotion in diving ducks: drag, buoyancy and acceleration in a size gradient of species. *J. Exp. Biol*., **159**, 89-108.

Webb, P. W. 1982. Locomotor patterns in the evolution of actinopterygian fishes. *Amer. Zool.*, **22**, 329-342

Lovvorn, J. R., Liggins, G. A., Borstad, M. H., Calisal, S. M., Mikkelsen, J. 2001. Hydrodynamic drag of diving birds: effects of body size, body shape and featheres at steady speeds. *J. Exp. Biol*., **204**, 1547-1557.

Mehranvar, L., Healey, L., Farrell, A., Hinch, S. 2004. Social versus genetic measures of reproductive success in sockeye salmon, *Oncorhynchus nerka*. *Evolutionary Ecology Research*, **6**, 1167-1181.

Miller, P. J. O., Johnson, M. P., Tyack, P. L. Terray, E. A. 2004. Swimming gaits, passive drag and buoyancy of diving sperm whales Physeter macrocephalus. *J. Exp. Biol*., **207**, 1953-1967

Mittal, R. 2004. Computational modeling in biohydrodynamics: trends, C

challenges, and recent Advances. *IEEE Journal of Oceanic Engineering*, **29**, 595-604

Munson, B. R., Young, D. F., Okiishi, T. H. 2006. Fundamentals of Fluid Mechanics (Fifth edition). John Wiley & Sons, Inc.

Obrecht, H. H., Pennycuick, C. J., Fuller, M. R. 1988. Wind tunnel experiments to assess the effects of back-mounted radio transmitters on bird body drag. *J. Exp. Biol*., **135**, 265-273.

OnlineCFD a. CFD Online: Dimensionless wall distance [Online]

http://www.cfd-online.com/Wiki/Dimensionless_wall_distance (27.05.09)

OnlineCFD b. CFD Online: Meshing [Online]

http://www.cfd-online.com/Wiki/Meshing (27.05.09)

OnlineCFD c. CFD Online: Reynolds averaged equations [Online]

http://www.cfd-online.com/Wiki/Introduction_to_turbulence/Reynolds_averaged_equations (27.05.09)

OnlineCFD d. CFD Online: Skin friction coefficient [Online] http://www.cfd-online.com/Wiki/Skin_friction_coefficient (27.05.09)

OnlineCFD e. CFD Online: Turbulence kinetic energy[Online] http://www.cfd-online.com/Wiki/Introduction_to_turbulence/Turbulence_kinetic_energy (27.05.09)

OnlineCFD f. CFD Online: Wall functions [Online] http://www.cfd-online.com/Wiki/Wall_functions (27.05.09)

OpenCFD 2008. OpenFOAM 1.5: The Open Source CFD Toolbox. User Guide. 2008. http://foam.sourceforge.net/doc/Guides-a4/UserGuide.pdf (27.05.09)

Panara, D., Porta, M., Schoenfeld, T. LES and URANS unsteady boundary layer strategies for pulsating and oscillating turbulent channel flow applications. http://www.cerfacs.fr/~cfdbib/repository/TR_CFD_06_69.pdf (27.05.09)

Pennycuick, C. J. 1988. Empirical estimates of body drag of large waterfowl and raptors. *J. Exp. Biol.*, **135**, 253-264

Puijalon, S., Bornette, G., Sagnes, P. 2005. Adaptations to increasing hydraulic stress: morphology, hydrodynamics and fitness of two higher aquatic plant species. *Journal of Experimental Botany*, **412 (56)**. 777-786

Quinn, T. P., Foote, C. J. 1994. The effects of body size and sexual dimorphism on the reproductive behaviour of sockeye salmon, Onchorhyncus nerka. Anim. Behav., 48, 751-756

Quinn, T. P., Kinnison, M. T. 1999. Size-selective and sex-selective predation by brown bears on sockeye salmon. *Oecologia*, **121**, 273-282.

Rand, P. S., Hinch, S. G. 1998. Swim speeds and energy use of upriver-migrating sockeye salmon (Onchorhynchus nerka): simulating metabolic power and assessing risk of energy depletion. *Can. J. Fish. Aquat. Sci.*, **55**, 1832-1841

Roland, A. 1985. NASA History Series: Model Research: SP-4103 Model Research. Volume 2 [Online] http://history.nasa.gov/SP-4103/app-f.htm (24.05.09)

Sagnes, P., Champagne, J-Y., Morel, R. 2000. Shifts in drag and swimming potential during grayling ontogenesis: relations with habitat use. *Journal of Fish Biology*, **57**,

52-68.Shelley, A. E., Vogel, S. 2000. Reorientation of daffodil (Narcissus: Amaryllidaceae) flowers in wind: drag reduction and torsional flexibility. *American Journal of Botany*, **87(1),** 29-32.

Standen, E. M., Hinch, S.G., Healey, M. C., Farrell, A. P. 2002. Energetic costs of migration through the Fraser River Canyon, British Columbia, in adult pink (Onchorhynchus gorbuscha) and sockeye (Oncorhynchus nerka) salmon as assessed by EMG telemetry. *Can. J. Fish. Aquat. Sci.*, **59**, 1809-1818.Stelle, L. L., Blake, R. W., Trites, A. W. 2000. Hydrodynamic drag in steller sea lions (Eumetopias Jubatus), *J. Exp. Biol.*, **203**, 1915-1923

Zhu, Q., Wolfgang, M. J., Yue, D. K. P., Triantafyllou, M. S. 2002. Three-dimensional flow structures and vorticity control in fish-like swimming. *J. Fluid Mech*., **468**, 1-28.

ToucanMuseum. Toucan Virtual Museum.

http://www.toucan.co.jp/ (27.05.09)

Triantafyllou, M. S., Triantafyllou, G. S., Yue, D. K. P. 2000. Hydrodynamics of Fishlike Swimming. *Annu. Rev. Fluid Mech*., **32**, 33-53.

VisualizationWiki. Visualization wiki: Streamlines [Online]

https://visualization.hpc.mil/wiki/Streamlines (24.05.09)

Vogel, S. 1994. Life in moving fluids. The physical biology of flow. Princeton University Press, Princeton. Wahidi, R., Chakroun, W., Al-Fahed, S. 2005. The behavior of the skin-friction coefficient of a turbulent boundary layer flow over a flat plate with differently configured transverse square grooves. *Experimental Thermal and Fluid Science*, **30-2**, 141-152

Wilcox, C. D. 2006. Turbulence Modeling for CFD. DCW Industries.

Wolfgang, M. J., Anderson, J. M., Grosengaug, M. A., Yue, D. K. P., Triantafyllou, M. S. 1999. Near-body flow dynamics in swimming fish. *J. Exp. Biol*., **202**, 2303-2327.

Wütrich, B. 2007. Simulation and validation of compressible flow in nozzle geometries and validation of OpenFOAM for this application. MSc thesis.

APPENDIX

APPENDIX A.

Here sockeye salmon models with varying aspect ratios are presented.

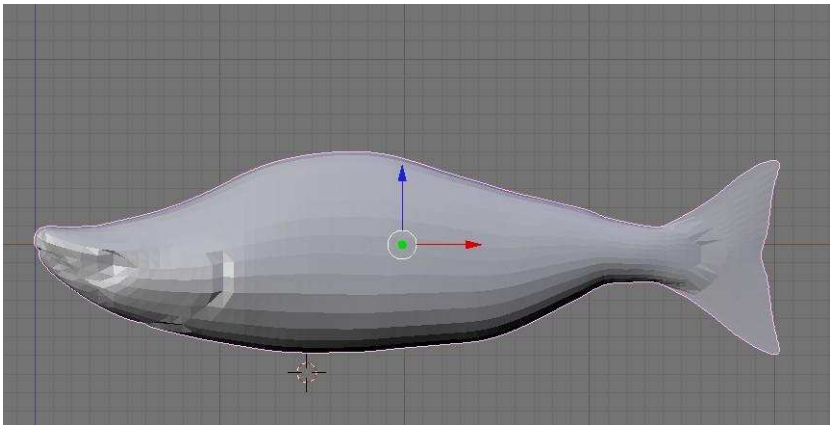

Figure 1. Sockeye model with aspect ratio 2.82.

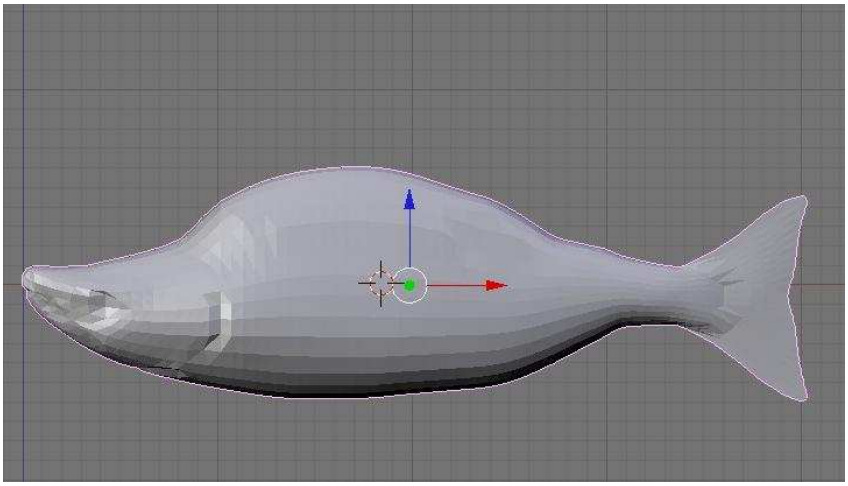

Figure 2. Sockeye model with aspect ratio 2.58.

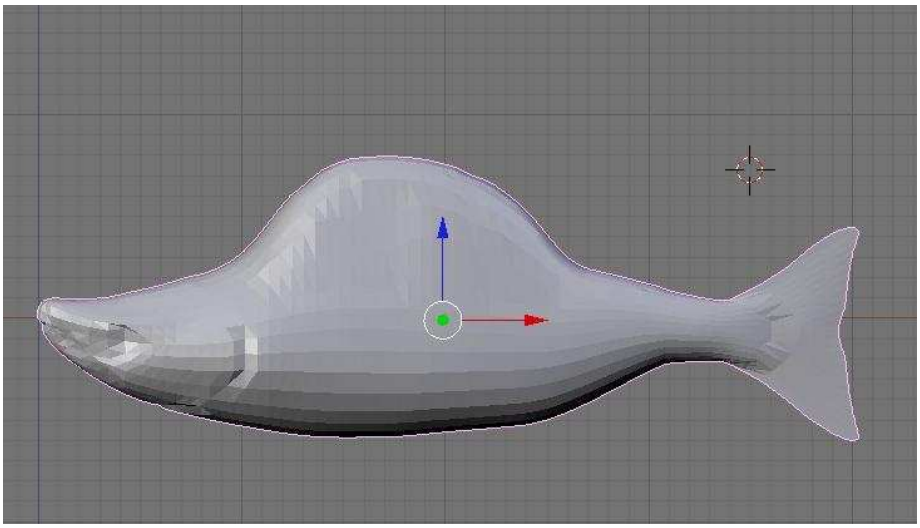

Figure 3. Sockeye model with aspect ratio 2.21.

APPENDIX B.

Here the relationships between drag force and drag coefficient on fish models and free-stream velocity.

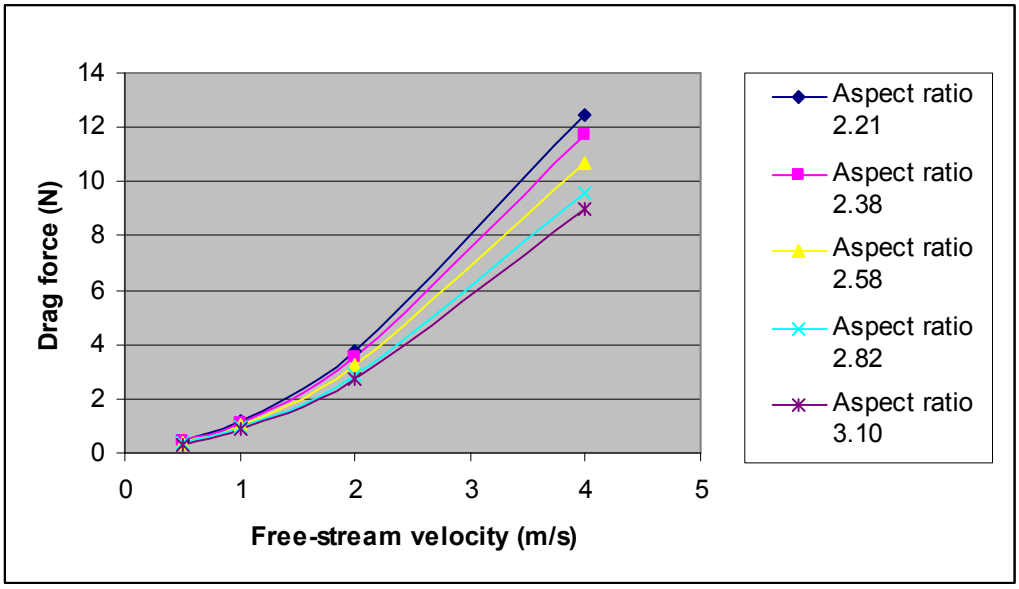

Figure 4. Drag force plotted against free-stream velocity.

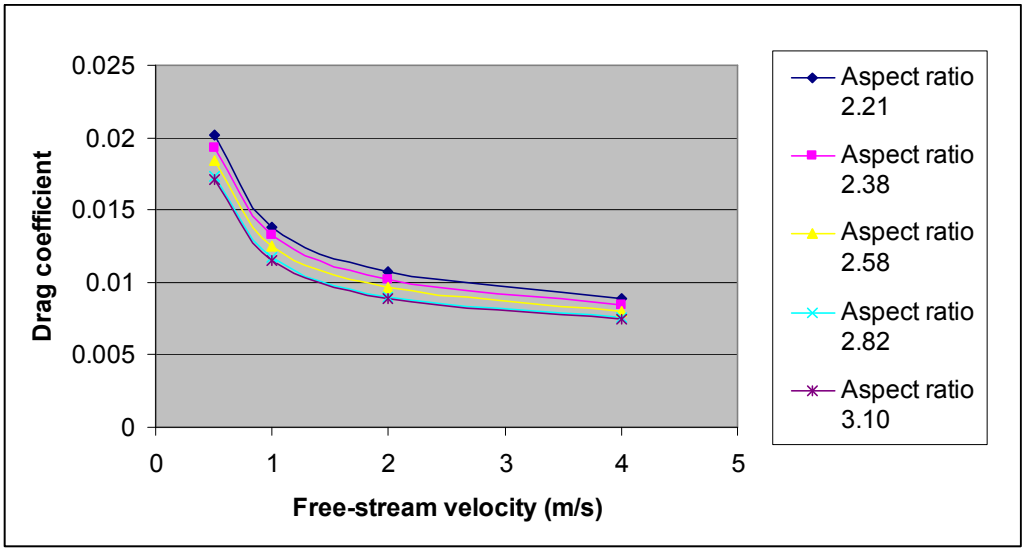

Figure 5. Drag coefficient plotted against free-stream velocity